Luminescence Properties and Energy Transfer of Tm3+-Eu3+ double Doped LiLaSiO4 Phosphors

Xiulan Wu
shaanxi university of science and technology
Liang Du (duliang199425@163.com)
Shaanxi University of Science and Technology Xi\'an Campus: Shaanxi University of Science and Technology https://orcid.org/0000-0002-1901-7377
Qiang Ren
shaanxi university of science and technology
Ou Hai
shaanxi university of science and technology

Research Article

Keywords: LiLaSiO4:yTm3+, zEu3+; Quantum yield; Energy transfer; Luminescent color

Posted Date: February 16th, 2021

DOI: https://doi.org/10.21203/rs.3.rs-192683/v1

Luminescence properties and energy transfer of Tm^{3+}-Eu^{3+} double doped $LiLaSiO_4$ phosphors

Xiulan Wu, Liang Du*, Qiang Ren, Ou Hai*

School of Materials Science and Engineering, Shaanxi Key Laboratory of Green Preparation and Functionalization for Inorganic Materials, Shaanxi University of Science and Technology, Xi'an, 710021, People's Republic of China

Abstract:

A series of $LiLaSiO_4$:yTm^{3+}, zEu^{3+} phosphors were prepared by high temperature solid-phase reaction. The microstructure, luminescence performance and quantum yield of the phosphors are characterized by XRD, SEM and fluorescence spectrometer. When the monitoring wavelength is 360 nm, $LiLaSiO_4$:yTm^{3+} phosphors showed a sharp emission peak at 460 nm, corresponding to the $^7F_0 \rightarrow {}^5D_2$ energy level transition, and the concentration quenching point of Tm^{3+} ions was y=0.015. When the monitoring wavelength is 360 nm, $LiLaSiO_4$:yTm^{3+}, zEu^{3+} phosphors have emission peaks of Tm^{3+} and Eu^{3+} ions at 460 and 618 nm, respectively. As the molar mass fraction of Eu^{3+} ions doped increases, the luminous intensity of Tm^{3+} ions gradually decrease, and the luminous intensity of Eu^{3+} ions increases first and then decreases, and the concentration quenching point of Eu^{3+} ions was z=0.08. The energy transfer of $Tm^{3+} \rightarrow Eu^{3+}$ ions through electric dipole- electric dipole interactions is demonstrated by the luminous intensity variation law and fluorescence lifetime. By changing the doping ratio of Eu^{3+}

* *Corresponding author. Tel: +86 15291196301*
E-mail address: duliang199425@163.com (L. Du), haiou@sust.edu.cn (O. Hai)

and Tb^{3+} ions, the full-color control of the phosphor luminescent color from blue to red can be achieved.

Keywords: $LiLaSiO_4:yTm^{3+}$, zEu^{3+}; Quantum yield; Energy transfer; Luminescent color

1. Introduction

The rapid development of solid-state lighting has made revolutionary progress in the field of lighting, providing a solid foundation for the global economy and energy security. Solid-state lighting products have many advantages such as high luminous efficiency, good durability and easy maintenance[1,2]. At present, the market generally uses yellow phosphor $YAG:Ce^{3+}$ to coat blue light-emitting LED chips to produce white light[3]. Although this method is simple and quick, it has disadvantages such as easy aging, low color rendering index and high color temperature[4]. In order to solve these problems, the sensitizer and the activator are co-doped into the same matrix to prepare a single matrix phosphor, which has the advantages of good stability, no phase separation, and simple preparation process[5,6]. In recent years, driven by the development of solid-state lighting w-LEDs, a variety of single matrix w-LEDs phosphors have appeared, and their luminous performance has also been improved[7].

Rare earth ions are shielded by the outer layers of 5s and 5p electrons, resulting in sharp spectral lines and high color purity in the 4f layer emission spectrum[8,9]. Because of its special 4f energy level structure, it can exhibit different electronic transition forms and rich energy level transition modes, so it can absorb or emit light of various wavelengths from ultraviolet to infrared[10]. It is known as “a treasure house

of luminescent materials", widely used in modern lighting, display, testing and biomedical diagnosis and other fields[11]. In rare earth ions, Eu3+ ions have the electron configurations of 4f6, 5s2 and 5p6. which can produce $^5D_0 \rightarrow ^7F_J$ (J=1,2,3,4) energy level transition under the excitation of ultraviolet light or cathode ray, and the main emission peak located in the red region, it is often used as a red emitting center[12,13]. The Russell-Saunders coupling in the 4f configuration of the rare earth Tm^{3+} ions has a strong deviation, resulting in complex energy levels and different energy level transition[14,15]. Therefore, the relaxation of the highly excited states of Tm^{3+} can occur through a large number of relaxation pathways. So produces infrared radiation, visible light and medium-intensity ultraviolet rays[16]. By doping Tm^{3+} ions in inorganic compounds and under appropriate ultraviolet light excitation, the $^1D_2 \rightarrow ^3F_4$ energy level transition of Tm^{3+} ions appear in the emission band of the blue region[17]. Doping Tm^{3+} ions in crystal and glass laser materials, the $^3H_4 \rightarrow ^3H_6$ energy level transition produces 1.9 nm laser emission, which can be used in medical treatment, and the $^3H_4 \rightarrow ^3F_4$ energy level transition produces 1.47 nm laser emission, which can be used in optical communication and fiber amplifier[18,19].

Silicate matrix has the advantages of low cost, stable physicochemical stability and environmental friendliness[20]. Most of the silicate phosphors have good absorption for near-ultraviolet chips or blue chips. The rich crystal structure not only provides a good basis for dimming, but also provides a variety of crystal field environments for rare earth ions, which in turn affects the luminescence performance of rare earth ions[21,22]. Wang et al[23]. studied tunable luminescence and energy

transfer in $Y_2BaAl_4SiO_{12}$:Tb^{3+},Eu^{3+} phosphors and found Tb^{3+} and Eu^{3+} double doped $Y_2BaAl_4SiO_{12}$ phosphor has the energy transfer from $Tb^{3+} \rightarrow Eu^{3+}$, realizing the adjustable luminescence from green to yellow and finally to red, with the highest energy transfer efficiency up to 67%. Li et al[24]. studied luminescence properties and energy transfer of Dy^{3+}/Tm^{3+} co-activated $SrCaAl_2SiO_7$ phosphor and found under the excitation of 350 nm, Tm^{3+}/Dy^{3+} co-activated $SrCaAl_2SiO_7$ phosphor emits white light. By properly adjusting the ratio of Tm^{3+}/Dy^{3+}, the light emission color can be changed from blue to yellow, including the white light area. The white light CCT is 5622 K, and the color coordinate value (0.3296, 0.3284) is close to the standard white light (0.33, 0.33). The structure of the $LiLaSiO_4$ compound is a very stable $[SiO_4]^{4-}$tetrahedron, in which silicon atoms occupy the center and four oxygen atoms occupy the four corners[25]. In the ultraviolet region, it has strong absorption and transfer to the activated ions, and then emits the characteristic light of the activated ions[26].

A series of Tm^{3+}/Eu^{3+} double doped $LiLaSiO_4$ fluorescent materials were synthesized by high temperature solid-phase reaction. The samples were analyzed and characterized by XRD, SEM, EDS and fluorescence spectrophotometer. Based on the principle of three primary colors, the panchromatic control of luminescent color from blue to red is realized by adjusting the relative concentration of Eu^{3+} and Tm^{3+} ions.

2. Experiment and characterization

2.1 Experimental process

A number of $LiLa_{1-y-z}SiO_4$:yTm^{3+}, zEu^{3+} (y and z are the molar mass fractions) phosphors were prepared by high temperature solid-reaction reaction. All the raw

materials used were purchased from lithium carbonate (Li_2CO_3, AR), silicon dioxide (SiO_2, AR), lanthanum oxide (La_2O_3, 99.99%), (Tm_2O_3, 99.99%), europium oxide (Eu_2O_3, 99.99%) produced by Sinopharm Chemical Reagent Shanghai Co., LTD. Weigh the raw materials according to their corresponding stoichiometric ratios, and then transfer them to an agate mortar for full grinding. Add a small amount of absolute ethanol during grinding to make the materials evenly ground, then put it into Al_2O_3 crucible and send it into the muffle furnace. Raise the temperature from room temperature to 850℃ for 8 hours. At this stage, moisture and CO_2 and other gases in the material can be removed. Then continue to heat up to 1175℃ for 8 hours. After the sample is naturally cooled, it will be fully ground into fine powder for characterization test.

2.2 Performance characterization

The phase composition of the sample was analyzed by the Japanese D/max2200PC X-ray diffractometer. The microstructure of the sample was measured on FEI Tecnai G2 20 TEM in the United States. The surface morphology of the samples was observed by high resolution field emission SEM of FEIVerios460 and analyzed qualitatively by EDS elements. The excitation and emission spectra data of the samples was obtained by Hitachi F-4600 fluorescence spectrometer. Fluorescence lifetime and quantum yield data was obtained at FS5 fluorescence spectrometer in Edinburgh, UK. The color coordinates of the sample is calculated by CIE1931 software.

3. Analysis and discussion

3.1 Phase analysis

Fig. 1 shows the XRD pattern of $LiLaSiO_4$:yTm^{3+}, zEu^{3+}. It can be seen from the figure that the diffraction peak of the sample when doped with Tm^{3+} and Eu^{3+} ions matches well with the standard card of LiLaSiO4 (JCPDS No.48-0006). The ionic radii of La^{3+}, Tm^{3+} and Eu^{3+} ions are 1.061 Å, 0.880 Å and 0.947 Å, respectively. Since Eu^{3+} and Tm^{3+} ions have the same valence as La^{3+} ions and the ionic radius is close, thus Eu^{3+} and Tm^{3+} ions replace La^{3+} ions sites in $LiLaSiO_4$. It was also found that the diffraction peaks of the samples as a whole are shifted toward a large angle, based on Bragg equation $2d\sin\theta = n\lambda$, when the dopant ions Tm^{3+} and Eu^{3+} ions occupy the position of La^{3+} ions in the matrix, resulting in a smaller crystal plane spacing and thus shifting the diffraction peaks toward a large angle.

Fig. 2 (a-b) shows SEM images of $LiLaSiO_4$:0.015Tm^{3+}, 0.08Eu^{3+} phosphor. It can be seen from the SEM images that the phosphors are like cylindrical spheres with regular morphology and uniform size. The surface morphology of the phosphors has a great influence on the luminescence. The cylindrical spherical shape not only has a higher packing density, and the dense particles reduce the light scattering loss to improve the luminescence efficiency, but also have a smaller force area, making the irregular luminescent layer minimize. The lattice stripes can be clearly seen in Fig. 2(c), indicating that the crystallization performance of the phosphors prepared under the experimental conditions is excellent, and the (112) crystal plane of $LiLaSiO_4$ corresponds to a crystal plane spacing of d=2.9411 Å. Fig. 2(d) shows the results of the qualitative analysis of the EDS in the region of Fig. 2(a). The analysis results showed that there were Si, O, La, Tm and Eu elements, and the content of Si, O and La elements

was significantly higher than that of Tm and Eu elements. Li is not found because of the beryllium window of the Si(Li) detector in the spectrometer limits the measurement of ultra-light elements. Fig. 2(e) shows the mapping of Si, O, La, Tm, and Eu elements in $LiLaSiO_4$:0.015Tm^{3+}, 0.08Eu^{3+} phosphor. It can be seen from the figure that the doped elements are uniformly distributed in the phosphors. Combined with the XRD analysis results in Fig. 1, it strongly proves that doping a small amount of Tm^{3+} and Eu^{3+} ions have little effect on the crystal structure of $LiLaSiO_4$.

3.3 Spectral discussion

The curve on the left side of Fig. 3 shows the excitation spectrum of $LiLaSiO_4$:0.015Tm^{3+} phosphor. When the monitoring wavelength is 460 nm, only has a sharp excitation peak at 360 nm, which corresponds to the $^3H_6 \rightarrow {}^1D_2$ energy level transition of the Tm^{3+} ions from the ground state to the excited state[27]. The curve on the right side of Fig. 3 shows the emission spectrum under the monitoring of 360 nm wavelength. It emits blue light at 460 nm, corresponding to the $^1D_2 \rightarrow {}^3F_4$ energy level transition of Tm^{3+} ions[28].

Fig. 4 shows the emission spectrum of $LiLaSiO_4$:yTm^{3+} (y=0.005, 0.01, 0.015, 0.02, 0.04 and 0.06) phosphors. When the monitoring wavelength is 360 nm, it can be seen from the figure that with the change of the molar mass fraction of doped Tm^{3+} ions, there is no significant change in the position and shape of the emission spectrum, only the luminous intensity changes significantly. As the molar mass fraction of Tm^{3+} ions increase from y=0.005, the luminous intensity continues to increase. When the molar mass fraction of doping y=0.015, the luminous intensity reaches the maximum, and

then the luminous intensity decreases due to the concentration quenching effect.

The occurrence of concentration quenching indicates that the excited Tm^{3+} ions energy has a non-radiative dissipation process. At higher concentrations, the energy transfer between Tm^{3+} ions are greatly increased, making the excited state energy more likely to be captured by the quenching center in the crystal lattice, and non-radiative transitions lose effective energy. According to reports in the literature, the energy transfer mechanism includes two categories: exchange interactions and electric multipole interactions[29]. Blasse formula (1) can be used to link the critical distance (R_C) with concentration quenching[30].

$$R_C = 2(\frac{3V}{4\pi X_C Z})^{1/3} \quad (1)$$

Where, V is the unit cell volume, X_C is the quenching concentration of the activator Tm^{3+} ions, and Z is the number of ions in the unit cell. In $LiLaSiO_4$ matrix, V=580.4 $Å^3$, Z=4, and X_C=0.015 were substituted into formula (1) to calculate that R_C=20.98 Å, which was much larger than 5 Å, and the Tm^{3+} ions concentration quenching was caused by electric multipole interaction[31].

According to the Dexter concentration quenching theory, the luminous intensity of Tm^{3+} ions and the molar mass fraction of Tm^{3+} ions can be expressed by formula (2)[32].

$$\frac{1}{y} = K[1 + \beta(y)^{Q/3}]^{-1} \quad (2)$$

Where y is the concentration of Tm^{3+} ions, K and β are constants under a given crystal, and θ=6, 8 or 10, respectively representing electric dipole-electric dipole interaction, electric dipole-electric quadrupole interaction, and electric quadrupole-

electric quadrupole interaction. Because $\beta(y)^{Q/3} \gg 1$, formula (2) is transformed into formula (3)[33].

$$\lg\left(\frac{I}{y}\right) = K - \frac{\theta}{3} lgy \quad (K = lgk - lg\beta) \tag{3}$$

In Fig. 5, $\lg\left(\frac{I}{y}\right) - \lg(y)$ is used as the coordinate axis to express the linear fitting of the doping point after concentration quenching. The slope of the linear fitting equation is Slope=-1.62439, so it can be calculated θ=4.87317≈6. This indicates that concentration quenching of Tm^{3+} ions is dominated by electric dipole-electric dipole interaction.

Fig. 6(a) shows the excitation and emission spectra of $LiLaSiO_4$:0.08Eu^{3+} phosphor. The excitation spectrum of the phosphor is composed of a series of peaks originating from the f-f transition of Eu^{3+} ions. The series of spikes are located at 362, 383, 395, 465, and 535 nm and are attributed to the $^7F_0 \rightarrow {}^5D_4$, $^7F_0 \rightarrow {}^5L_7$, $^7F_0 \rightarrow 5L_6$, $^7F_0 \rightarrow {}^5D_3$, and $^7F_0 \rightarrow {}^5D_2$ energy level transitions of Eu^{3+} ions, respectively[34]. The main excitation peak is at 395 nm. Therefore, $LiLaSiO_4$:0.08Eu^{3+} phosphor can be effectively excited by near-ultraviolet light. Under the monitoring of 395 nm wavelength, the emission spectrum of $LiLaSiO_4$:0.08Eu^{3+} consists of four characteristic emission peaks located at 598($^5D_0 \rightarrow {}^7F_1$), 618 ($^5D_0 \rightarrow {}^7F_2$), 654 ($^5D_0 \rightarrow {}^7F_3$) and 707 nm($^5D_0 \rightarrow {}^7F_4$)[35]. The main peak is located at 618 nm, and its intensity is much higher than that of other emission peaks. Based on the parity selection rule, when Eu^{3+} ions occupy the center of inversion symmetry in crystal lattice, the $^5D_0 \rightarrow {}^7F_1$ energy level transition radiation is dominant, if it is not in the inversion center, $^5D_0 \rightarrow {}^7F_2$ energy level transition radiation is dominant. The main emission peak of $LiLaSiO_4$:0.08Eu^{3+} phosphor was derived from

$^5D_0 \rightarrow {}^7F_2$ transition, indicating that Eu^{3+} ions mainly occupied the lattice of non-inversion center in the matrix lattice[36]. Fig. 6(b) shows the emission spectra of $LiLaSiO_4:0.08Eu^{3+}$ phosphors under different monitoring wavelengths (λ_{ex}=362,383,395,465 and 535 nm). It can be found from the figure that all emission peaks have the same shape and position, but the luminous intensity is different, and the magnitude of the luminous intensity corresponds to the intensity of the excitation peak.

Fig. 7(a) shows the excitation spectrum of $LiLaSiO_4:0.08Eu^{3+}$ phosphor on the left and the emission spectrum of $LiLaSiO_4:0.015Tm^{3+}$ phosphor on the right. According to Dexter theory, effective energy transfer requires that the excitation spectrum of Eu^{3+} ions and the emission spectrum of Tm^{3+} ions overlap partially. When the main emission peak of Eu^{3+} ions is used as the monitoring wavelength, the excitation spectrum should have a characteristic excitation peak of Tm^{3+} ions. It can be clearly seen from Fig. 7(a) that the excitation spectrum of Eu^{3+} ions and the emission spectrum of Tm^{3+} ions partially overlap between 450～480 nm. So the first condition of Dexter energy transfer is satisfied. Fig. 7(b) shows the excitation and emission spectra of $LiLaSiO_4:0.015Tm^{3+}$, $0.08Eu^{3+}$ phosphor. When the monitoring wavelength is 360 nm, the emission spectrum of $LiLaSiO_4:0.015Tm^{3+}$, $0.08Eu^{3+}$ phosphor not only shows a characteristic emission peak of Tm^{3+} ions at 460 nm, but also a characteristic emission peak of Eu^{3+} ions at 618 nm. When the monitoring wavelength is 395 nm, only shows a characteristic emission peak of Eu^{3+} ions at 618 nm. When the monitoring wavelength is 618 nm, the excitation spectrum not only shows the characteristic excitation peak of Tm^{3+} ions at 360 nm, but also the characteristic excitation peak of Eu^{3+} ions at 395 nm. When the monitoring

wavelength is 460 nm, only shows a characteristic excitation peak Tm^{3+} ions at 360 nm. So the second condition of Dexter energy transfer is satisfied. Therefore, there is the possibility of Tm^{3+}→Eu^{3+} energy transfer in $LiLaSiO_4$:yTm^{3+}, zEu^{3+} phosphors.

Fig. 8 shows the emission spectrum of the $LiLaSiO_4$:0.015Tm^{3+}, zEu^{3+} sample (z=0.02, 0.04, 0.06, 0.08 and 0.10). It can be seen from the figure that the molar mass fraction of Eu^{3+} ions doping has a greater impact on the luminous intensity of the phosphors. With the increase of the doped molar mass fraction of Eu^{3+} ions, the luminous intensity of Tm^{3+} ions decrease gradually, while the luminous intensity of Eu^{3+} ions increases first and then decreases. When the doping molar mass fraction of Eu^{3+} ions is z=0.08, the luminous intensity of Eu^{3+} reaches the strongest, and then the concentration quenching causes the luminous intensity of Eu^{3+} ions to decrease. This is because when the Eu^{3+} ions doping molar mass fraction in phosphors is too large, there is a cross-relaxation process between the ions, which leads to the quenching of high energy level luminescence. In addition, since the molar mass fraction of Tm^{3+} ions doping is fixed, the luminous intensity of Tm^{3+} ions decreases with the increase of the molar mass fraction of Eu^{3+} ions doping, which is caused by the existence of Tm^{3+}→Eu^{3+} energy transfer.

3.4 Fluorescence lifetime

Fig. 9(a) shows the fluorescence decay curve of $LiLaSiO_4$:0.015Tm^{3+}, zEu^{3+} phosphor at 460 nm when the monitoring wavelength is 360 nm. The curve is fitted by the double exponential function (4)[37].

$$I_t = A_1 exp\left(-t/\tau_1\right) + A_2 exp\left(-t/\tau_2\right) \quad (4)$$

In formula (4), I_t refers to the luminous intensity at time t, A_1 and A_2 are the fitting parameters, τ_1 and τ_2 are the fast and slow lifetimes fitted in the exponential part, and t refers to the time. Calculate the average fluorescence lifetime by formula (5)[38].

$$\tau_{av} = \frac{A_1\tau_1^2+A_2\tau_2^2}{A_1\tau_1+A_2\tau_2} \quad (5)$$

Fig. 9(b) shows the change curve of fluorescence lifetime and all the calculated results are listed in Table 1. It can be seen that as the Eu^{3+} ions molar mass fraction z increases from 0 to 0.1, the fluorescence lifetime slowly decreases from 0.0161ms to 0.0085ms. This is because with the increase of the molar mass fraction of Eu^{3+}, the Tm^{3+}→Eu^{3+} ion spacing gradually shortens, and the interaction gradually increases, so the fluorescence lifetime of Tm^{3+} ions decreases continuously. This is consistent with the change of luminous intensity of Tm^{3+} ions in Fig. 8.

3.5 Tm3+→Eu3+ energy transfer

According to formula (6), luminous intensity data were used to calculate the energy transfer efficiency between Tm^{3+}→Eu^{3+}[39].

$$\eta_{ET} = 1 - \frac{I_S}{I_{S0}} \quad (6)$$

Where I_S is the luminous intensity of Tm^{3+} ions in the presence of Eu^{3+} ions, and I_{S0} is the luminous intensity of Tm^{3+}ions in the absence of Eu^{3+} ions. The energy transfer efficiency in Fig. 10 shows that as the Eu^{3+} ions doping molar mass fraction increases, the Tm^{3+}→Eu^{3+} energy transfer efficiency gradually increases. When the Eu^{3+} ions doping molar mass fraction is z=0.1, the transfer efficiency reaches the highest η_{ET} =68.01%.

Normally, the energy transfer from the sensitizers to the activators is achieved

through exchange interactions and electric multipole interactions. Whether energy transfer undergoes electric multipole interactions depends on the critical distance (R_C) between the sensitizers and activators. When R_C is greater than 5 Å, electric multipole interactions occurs. In 3.3, R_C=20.98Å has been calculated, indicating that the possibility of energy transfer through exchange interaction is very small. In this case, electric multipole interactions play a major role. According to the Dexter energy level transfer of the electric multipole interactions, the relationship (7) is given[40].

$$\frac{I_{S0}}{I_S} \approx \frac{\eta_0}{\eta} \propto C^{n/3} \quad (7)$$

Where η_0 and η are the quantum efficiency of Tm^{3+} ions in the absence and presence of Eu^{3+} ions, respectively, and the value of η_0/η can be calculated by the ratio of luminous intensity (I_{S0}/I_S), C is the total concentration of Tm^{3+} and Eu^{3+} ions, n=6, 8 or 10 correspond to electric dipole-electric dipole, electric dipole-electric quadrupole, or electric quadrupole-electric quadrupole interactions, respectively[41]. By comparing the values of the fitting factor R^2, the optimal linear relationship between I_{S0}/I_S and $C^{n/3}$ was obtained from Fig. 11, that is, n=6, R^2=0.95238, indicating that the energy transfer from Tm^{3+}→Eu^{3+} follows the electric dipole-electric dipole interaction.

3.6 Quantum yield

Fig. 12 is the use of the reference method to determine the standard material $BaSO_4$ and the test sample $LiLaSiO_4$:0.015Tm^{3+},0.08Eu^{3+} fluorescence integrated intensity, and compare the integrated intensity of the emitted light ($\int L_S$) and the integrated intensity difference of the absorbed light ($\int E_R$-) $\int E_S$), to obtain the fluorescence internal quantum efficiency QY, which can be calculated by formula (8)[42].

$$\eta_{QY} = \frac{\int L_S}{\int E_R - \int E_S} \quad (8)$$

When the monitoring wavelength is 360 nm, the absolute quantum yield of $LiLaSiO_4$:0.015Tm^{3+}, 0.08Eu^{3+} was 38.8%.

3.7 Color coordinates

Because people have subjective differences in color judgment, it is necessary to use scientific methods to accurately measure the color. The luminescent color is usually described by the CIE coordinate diagram. By importing the emission spectrum data of $LiLaSiO_4$:yTm^{3+}, zEu^{3+} into the CIE1931 software. It can be seen from Fig. 14 (a) that the color coordinates of $LiLaSiO_4$:0.08Eu^{3+} phosphors under different monitoring wavelengths are located in the red region. It can be seen from Fig. 14(b) that the color coordinates of $LiLaSiO_4$:yTm^{3+}, zEu^{3+} phosphors gradually transition from blue to red as the mole mass fraction of doped Eu^{3+} ions increase, realizing the regulation of phosphor luminescent color, and all the calculation results are listed in Table 2.

4. Conclusion

In summary, a series of $LiLaSiO_4$:yTm^{3+}, zEu^{3+} phosphors were prepared by high-temperature solid-phase reaction. The phosphor has high phase purity and excellent crystallization property, and its morphology is like cylindrical spheres. The phosphor can be effectively excited by near-ultraviolet light. Under the monitoring of 360 nm wavelength, $LiLaSiO_4$:yTm^{3+} phosphors appears Tm^{3+} ions $^7F_0 \rightarrow {}^5D_2$ energy level transition at 460 nm. The optimal doping amount of Tm^{3+} ion is y=0.015. $LiLaSiO_4$:yTm^{3+}, zEu^{3+} phosphors have emission peaks of Tm^{3+} and Eu^{3+} ions at 460 nm and 618 nm, respectively. As the molar mass fraction of Eu^{3+} ions doped increases,

the Tm^{3+} ions luminous intensity gradually decreases, and the Eu^{3+} ions luminous intensity first increases and then decreases, The optimal doping molar mass fraction of Eu^{3+} ions is z=0.08. It is proved that the electric dipole-electric dipole interaction leads to the energy transfer of Tm^{3+}→Eu^{3+} through the change of Tm^{3+} and Eu^{3+} ions luminous intensity and the change of Tm^{3+} ions fluorescence lifetime. The maximum transfer efficiency is η_{ET}=68.01%. The quantum yield QY=38.8%. By changing the doping ratio of Eu^{3+} and Tb^{3+} ions, the intensity of characteristic emission peaks of Eu^{3+} and Tb^{3+} ions can be changed, so as to realize panchromatic control of luminescent color from blue to red. $LiLaSiO_4$:yTm^{3+}, zEu^{3+} phosphors have regular morphology and tunable luminescence characteristics, indicating that it has potential application prospects in lighting, display, detection and other fields.

Acknowledgements

This work was financially supported by the Innovation of Science and Technology Plan Projects of Shaanxi Province, China (Grant No. 2013KTDZ03-02-01, 2017TSCXL-GY-07-02), Natural Science Foundation of Shaanxi Province (Grant No. 2019JQ-785), Research Starting Foundation from Shaanxi University of Science and Technology (Grant No. 2016BJ-41), and the Graduate Innovation Fund of Shaanxi University of Science and Technology (Grant No. SUST-A04).

References：

1. K. Thomas, D. Alexander, K. P. Mani, S. Gopi, S. Ajeesh Kumar, P. R. Biju, N. V. Unnikrishnan, and C. Joseph, J. Phys. Chem. Solids **137**, 109212 (2020).

2. J. Yang, H. Xiong, J. Dong, C. Yang, S. Gan, and L. Zou, J. Phys. Chem. Solids **111**, 355 (2017).

3. J. C. A. Santos, E. P. Silva, D. V. Sampaio, D. C. Silva, N. R. S. Souza, C. Kucera, J. Ballato, and R. S. Silva, J. Eur. Ceram. Soc. **40**, 3673 (2020).

4. X. KONG, Z. HE, and R. LIANG, J. Rare Earths **34**, 972 (2016).

5. J. Zhong, D. Chen, Y. Zhou, Z. Wan, M. Ding, and Z. Ji, J. Eur. Ceram. Soc. **36**, 1705 (2016).

6. J. Chen, Y. Tang, X. Yi, Y. Tian, D. Zhao, H. Lin, and S. Zhou, J. Eur. Ceram. Soc. **40**, 5852 (2020).

7. R. S. Yadav and S. B. Rai, J. Phys. Chem. Solids **114**, 179 (2018).

8. L. Vijayalakshmi, K. N. Kumar, and P. Hwang, Scr. Mater. **187**, 97 (2020).

9. X. Zhang, J. Zhang, and Y. Chen, Dye. Pigment. **149**, 696 (2018).

10. G. A. Sobral, M. A. Gomes, J. F. M. Avila, J. J. Rodrigues, Z. S. Macedo, J. M. Hickmann, and M. A. R. C. Alencar, J. Phys. Chem. Solids **98**, 81 (2016).

11. L. Sun, J. Liang, S. Wang, Q. Sun, B. Devakumar, and X. Huang, Mater. Today Energy **17**, 100487 (2020).

12. N. Guo, Y. Pan, W. Lv, R. Ouyang, and B. Shao, Opt. Laser Technol. **123**, 105938 (2020).

13. H. Yu, X. Shi, L. Huang, X. Kang, and D. Pan, J. Lumin. **225**, (2020).

14. W. Zhao, S. An, B. Fan, and S. Li, J. Lumin. **143**, 71 (2013).

15. Y. Zhai, Q. Sun, S. Yang, X. Zhao, T. Li, and H. Wang, Optik (Stuttg). **174**, 600 (2018).

16. L. Yang, Q. Liu, H. Zheng, S. Zhou, and W. Zhang, J. Phys. Chem. Solids **124**, 151 (2019).

17. N. Kucuk, Ü. H. Kaynar, S. Akca, Y. Alajlani, L. Yin, Y. Wang, J. Garcia Guinea, K. Bulcar, T. Dogan, Y. Karabulut, M. Ayvacikli, A. Canimoglu, M. Topaksu, and N. Can, J. Alloys Compd. **838**, 155587 (2020).

18. L. Li, M. Dou, Y. Yan, Y. Li, F. Ling, S. Jiang, G. Xiang, J. Liu, and X. Zhou, Opt. Mater. (Amst). **102**, 3 (2020).

19. J. Huang, W. You, G. Gong, G. Liu, P. Liu, and B. Wang, Opt. Mater. (Amst). **88**, 534 (2019).

20. C. Jin, J. Zhang, W. Lu, and Y. Fei, J. Lumin. **214**, (2019).

21. R. Mohan P, S. K. Jose, A. George, N. V. Unnikrishnan, C. Joseph, and P. R. Biju, J. Phys. Chem. Solids **119**, 166 (2018).

22. D. Rehani, S. Bishnoi, M. Saxena, D. Haranath, V. Gupta, and S. N. Sharma, J. Phys. Chem. Solids **143**, 109460 (2020).

23. J. Wang, X. Peng, D. Cheng, Z. Zheng, and H. Guo, J. Rare Earths (2020).

24. Y. Li, X. Wang, W. Liu, C. Wang, and Y. Wang, Mater. Res. Bull. **76**, 273 (2016).

25. J. Sun, X. Zhang, and R. Zhang, Mater. Lett. **267**, 127559 (2020).

26. S. Ullah, D. Zhong, Y. Feng, C. Dou, S. Sun, H. Kong, F. Zheng, Z. Wang, Y. Yin, J. Tang, and B. Teng, J. Phys. Chem. Solids **144**, 109485 (2020).

27. C. Wang, J. Jiang, S. Xin, Y. Shi, and G. Zhu, J. Lumin. **214**, 116521 (2019).

28. D. Zhu, C. Wang, and F. Jiang, J. Rare Earths **36**, 346 (2018).

29. Y. R. Parauha, R. S. Yadav, and S. J. Dhoble, Opt. Laser Technol. **124**, 105974 (2020).

30. J. Zhou and Z. Xia, Opt. Mater. (Amst). **53**, 116 (2016).

31. S. Liu, Y. Liang, Y. Zhu, X. Wu, R. Xu, M. Tong, and K. Li, Opt. Laser Technol. **84**, 1 (2016).

32. Y. Zhang, S. Hu, Y. Liu, Z. Wang, W. Ying, G. Zhou, and S. Wang, J. Eur. Ceram. Soc. **39**, 584 (2019).

33. T. Zhou, L. Mei, Y. Zhang, L. Liao, H. Liu, and Q. Guo, Opt. Laser Technol. **111**, 191 (2019).

34. Z. W. Zhang, Y. N. Wu, X. H. Shen, Y. J. Ren, W. G. Zhang, and D. J. Wang, Opt. Laser Technol. **62**, 63 (2014).

35. Y. Wu, M. Chen, K. Qiu, W. Zhang, and Q. Tang, Opt. Laser Technol. **118**, 20 (2019).

36. Y. Jiao, X. Wu, Q. Ren, O. Hai, F. Lin, and W. Bai, Opt. Laser Technol. **109**, 470 (2019).

37. C. Jin and J. Zhang, Opt. Laser Technol. **115**, 487 (2019).

38. A. Fu, A. Guan, F. Gao, X. Zhang, L. Zhou, Y. Meng, and H. Pan, Opt. Laser Technol. **96**, 43 (2017).

39. N. Deopa, S. Kaur, A. Prasad, B. Joshi, and A. S. Rao, Opt. Laser Technol. **108**, 434 (2018).

40. X. Wu, Y. Jiao, Q. Ren, O. Hai, F. Lin, H. Li, and W. Bai, Opt. Laser Technol. **108**, 456 (2018).

41. X. Wu, W. Bai, O. Hai, Q. Ren, J. Zheng, and Y. Ren, Opt. Laser Technol. **115**, 176 (2019).

42. X. Wu, W. Bai, O. Hai, Q. Ren, F. Lin, and Y. Jiao, Opt. Laser Technol. **107**, 46 (2018).

Figure captions:

Fig. 1 X-ray diffraction patterns of $LiLaSiO_4:yTm^{3+}$, zEu^{3+} phosphors and the standard card of $LiLaSiO_4$ (JCPDS NO. 48-0006).

Fig. 2 （a-b）SEM images of $LiLaSiO_4:0.015Tm^{3+},0.08Eu^{3+}$ phosphor, (c) TEM of $LiLaSiO_4:0.015Tm^{3+},0.08Eu^{3+}$ phosphor, (d) EDS of $LiLaSiO_4:0.015Tm^{3+},0.08Eu^{3+}$ phosphor, (e) element distribution of $LiLaSiO_4:0.015Tm^{3+},0.08Eu^{3+}$ phosphor.

Fig. 3 Excitation spectra and Emission spectra of $LiLaSiO_4:0.015Tm^{3+}$ phosphor.

Fig. 4 Emission spectra of $LiLaSiO_4:yTm^{3+}$ phosphor.

Fig. 5 $\lg\left(\frac{I}{y}\right) - \lg(y)$ relationship of Tm^{3+} ions in $LiLaSiO_4:yTm^{3+}$ phosphor

Fig. 6 (a) Excitation and emission spectra of $LiLaSiO_4:0.08Eu^{3+}$ phosphor, (b) emission spectra of $LiLaSiO_4:0.08Eu^{3+}$ phosphor at different monitoring wavelength (λ_{ex}=362, 383, 395 465 and 535nm)

Fig. 7 (a) Excitation spectra of $LiLaSiO_4:0.08Eu^{3+}$ phosphor and emission spectra of $LiLaSiO_4:0.015Tm^{3+}$ phosphor, (b) excitation and emission spectra of $LiLaSiO_4:0.015Tm^{3+}$, $0.08Eu^{3+}$ phosphor.

Fig. 8 Emission spectra of $LiLaSiO_4:0.015Tm^{3+}$, yEu^{3+} phosphors.

Fig. 9 (a) Decay curves of $LiLaSiO_4:0.015Tm^{3+}$, yEu^{3+} phosphors, (b)variation in decay times of phosphors with different Eu^{3+} doping rates.

Fig. 10 Energy transfer efficiency of $Tm^{3+}\rightarrow Eu^{3+}$ and changes in luminous intensity of Tm^{3+} and Eu^{3+} ions

Fig. 11 Fitting relationship of I_{S0}/I_S of Tm^{3+} on (a) $C(Tb^{3+}+Eu^{3+})^{6/3}$, (b) $C(Tb^{3+}+Eu^{3+})^{8/3}$ and (c)$C(Tb^{3+}+Eu^{3+})^{10/3}$.

Fig. 12 Excitation and emission spectra of $LiLaSiO_4$:0.015Tm^{3+}, 0.08Eu^{3+} phosphor reference sample for QY measurement

Fig. 13 (a) Color coordinates of $LiLaSiO_4$:0.08Eu^{3+} phosphors at different monitoring wavelength (λ_{ex}=362, 383, 395 465 and 535nm), (b) color coordinates of $LiLaSiO_4$:0.015Tm^{3+}, yEu^{3+} phosphors,

.

Table 1
The value of average lifetime (τ_{av}) of $LiLaSiO_4:yTm^{3+}$, zEu^{3+} phosphors.

N0.	Sample compositions	A_1	τ_1(ms)	A_2	τ_2(ms)	τ_{av}(ms)
1	$LiLaSiO_4:0.015Tm^{3+}$	36410.05	0.0131	4238.86	0.0283	0.0161
2	$LiLaSiO_4:0.015Tm^{3+},0.02Eu^{3+}$	31065.74	0.0108	5904.55	0.0245	0.0149
3	$LiLaSiO_4:0.015Tm^{3+},0.04Eu^{3+}$	23632.30	0.0097	3323.70	0.0239	0.0135
4	$LiLaSiO_4:0.015Tm^{3+},0.06Eu^{3+}$	20107.94	0.0074	3973.52	0.0196	0.0116
5	$LiLaSiO_4:0.015Tm^{3+},0.08Eu^{3+}$	19245.68	0.0064	1779.42	0.0205	0.0096
6	$LiLaSiO_4:0.015Tm^{3+},0.10Eu^{3+}$	18853.62	0.0061	1395.15	0.0190	0.0085

Table2

The color coordinate of $LiLaSiO_4:yTb^{3+}$, zEu^{3+} phosphors.

No.	Sample compositions	CIE coordinates (x, y)
A	**$LiLaSiO_4:0.015Tm^{3+}$**	**（0.139,0.046）**
B	**$LiLaSiO_4:0.015Tm^{3+},0.02Eu^{3+}$**	**(0.258,0.205)**
C	**$LiLaSiO_4:0.015Tm^{3+},0.04Eu^{3+}$**	**(0.386,0.272)**
D	**$LiLaSiO_4:0.015Tm^{3+},0.06Eu^{3+}$**	**(0.428,0.296)**
E	**$LiLaSiO_4:0.015Tm^{3+},0.08Eu^{3+}$**	**(0.463,0.313)**
F	**$LiLaSiO_4:0.015Tm^{3+},0.10Eu^{3+}$**	**(0.475,0.321.)**
G	**$LiLaSiO_4:0.08Eu^{3+}$**	**(0.656,0.344)**

Fig. 1 L. Du et al.

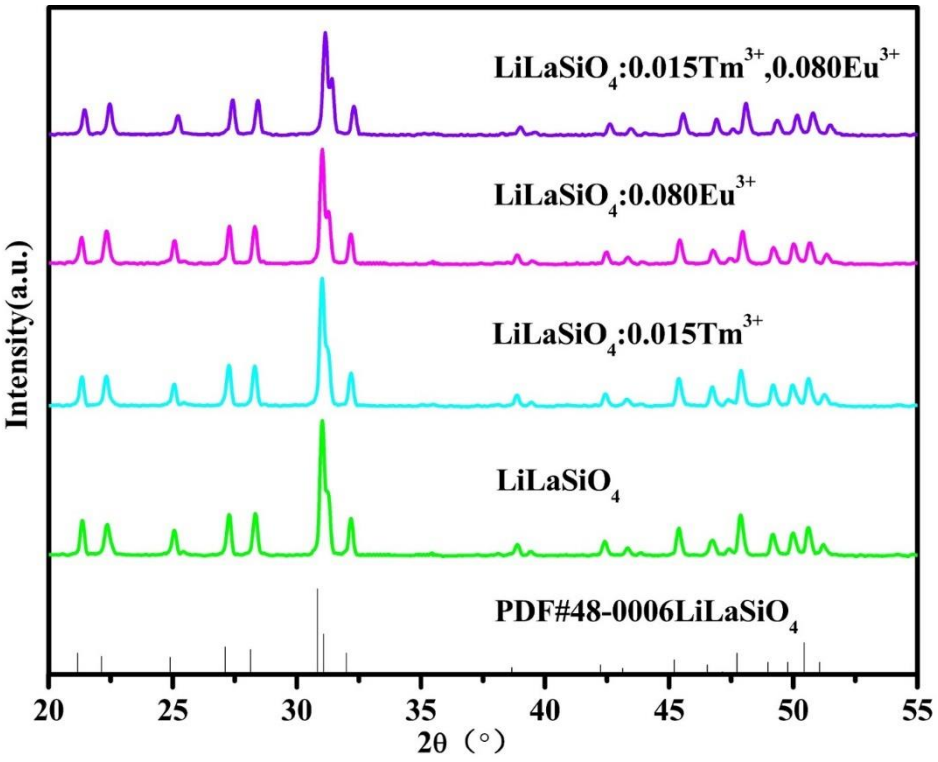

Fig. 2 L. Du et al.

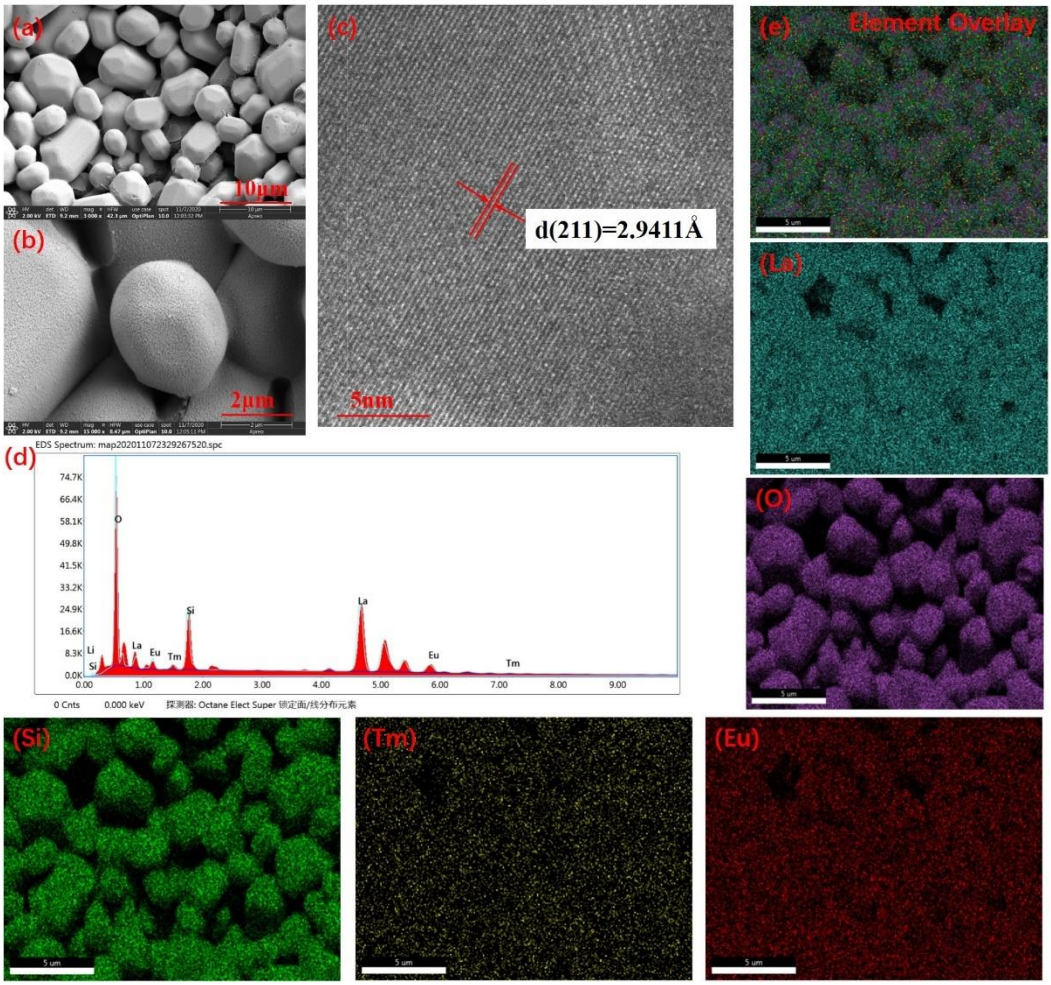

Fig. 3 L. Du et al.

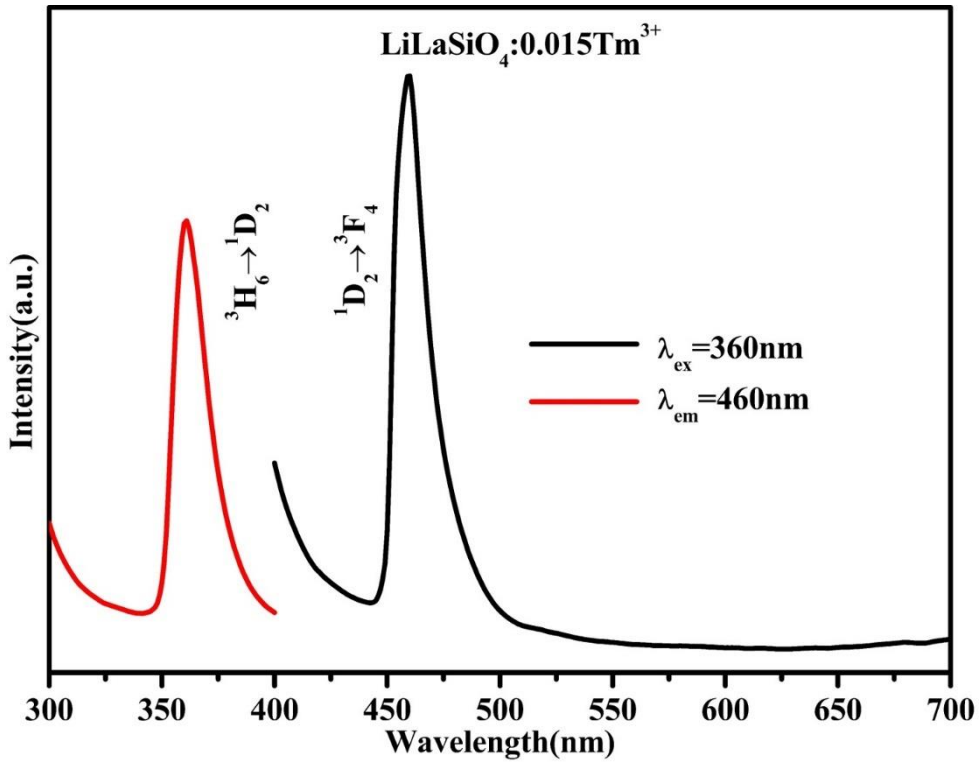

Fig. 4 L. Du et al.

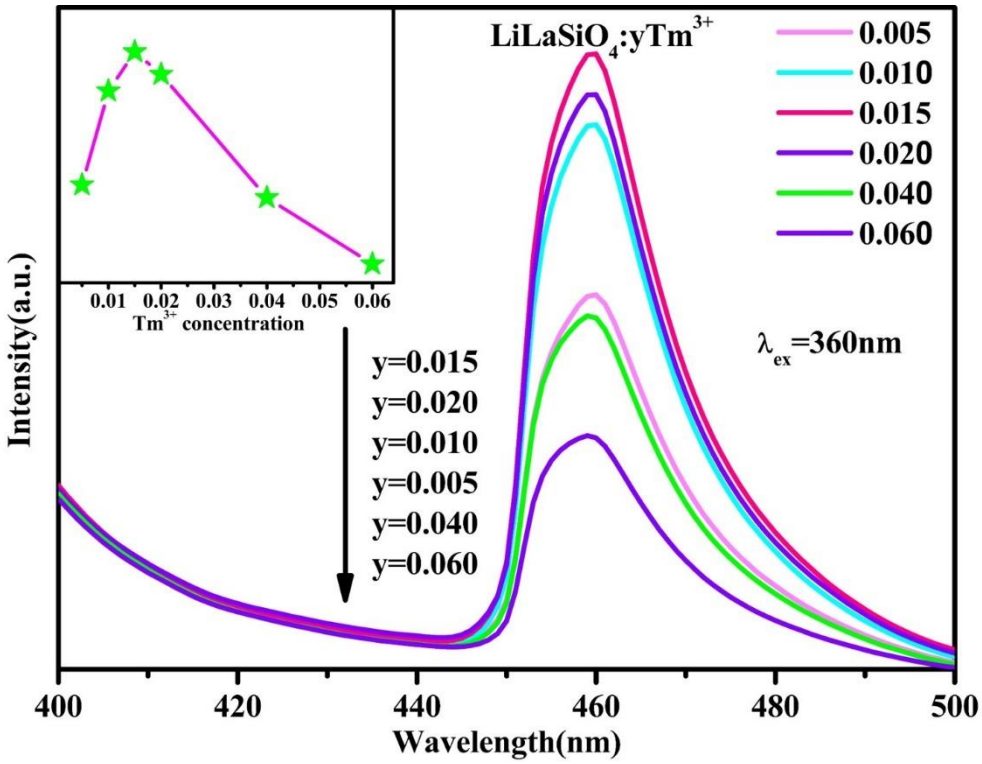

Fig. 5 L. Du et al.

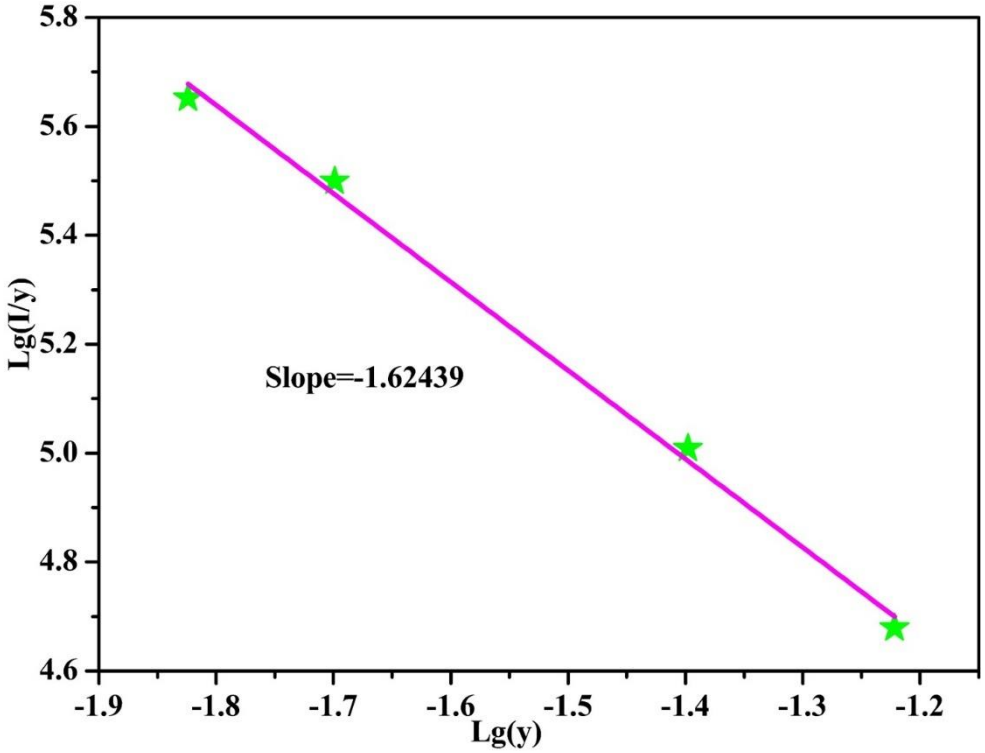

Fig. 6 L. Du et al.

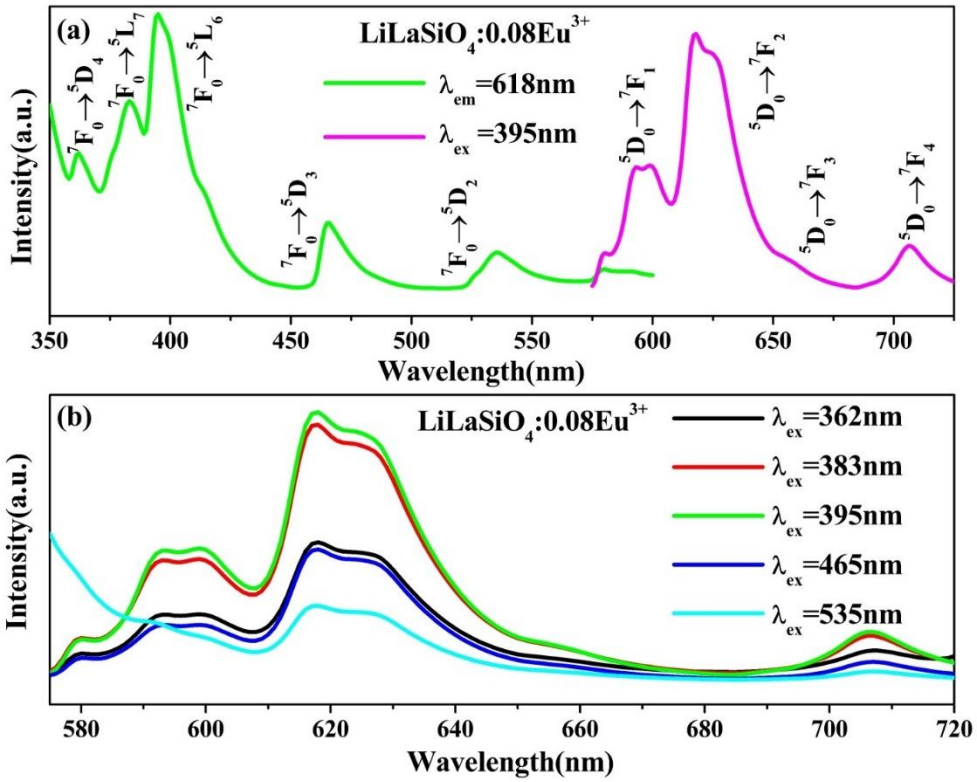

Fig. 7 L. Du et al.

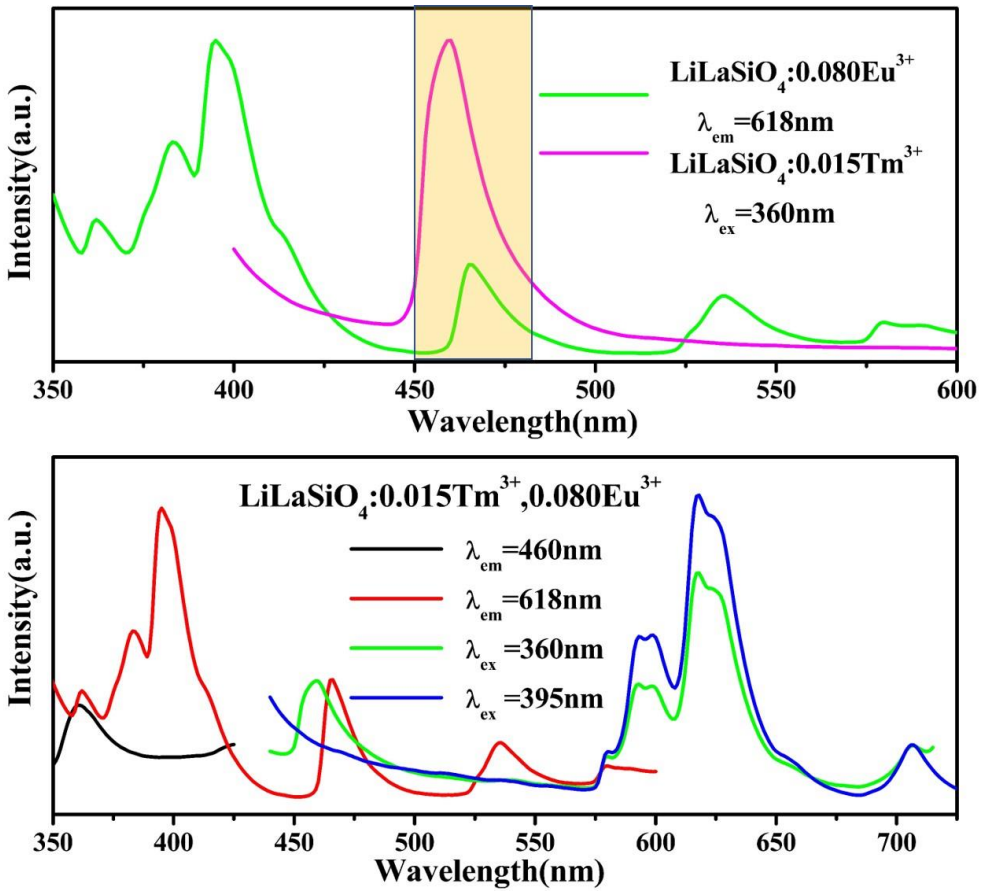

Fig. 8 L. Du et al.

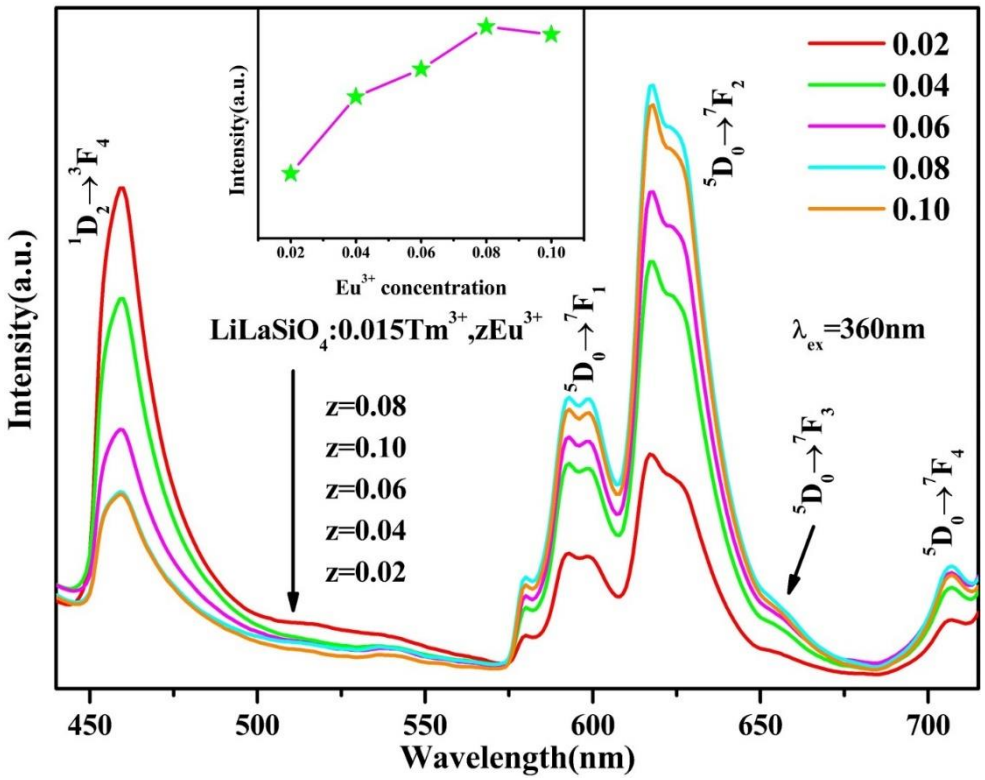

Fig. 9 L. Du et al.

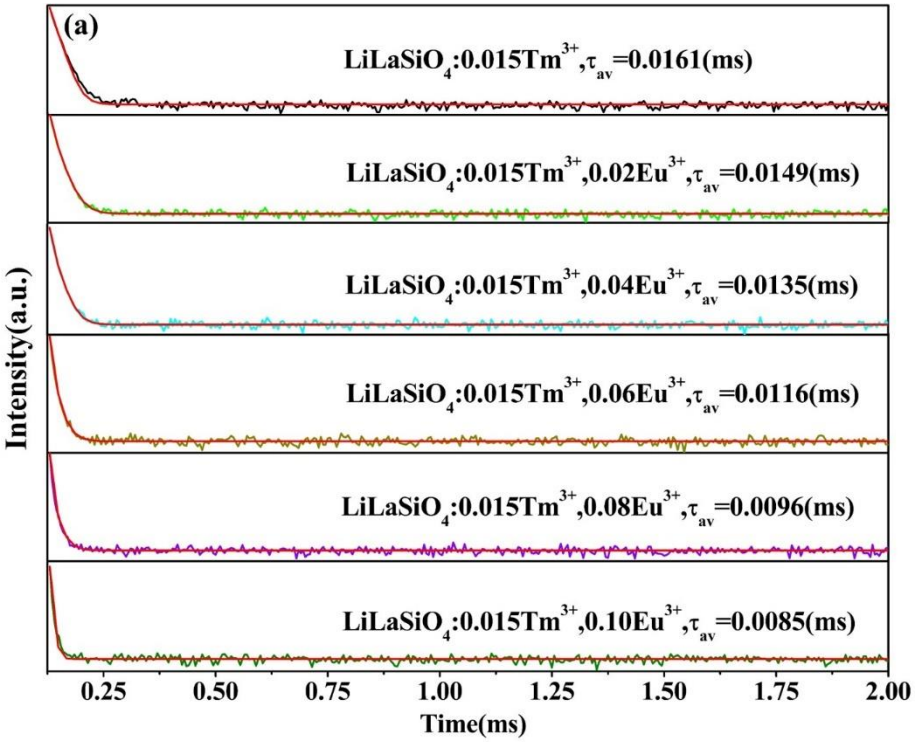

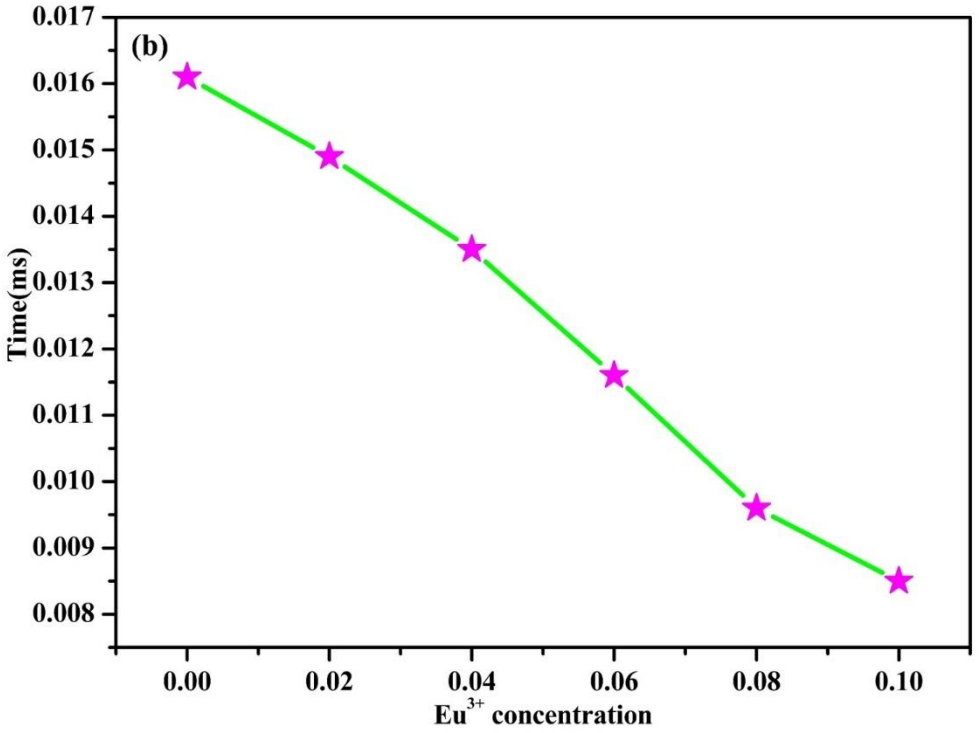

Fig. 10 L. Du et al.

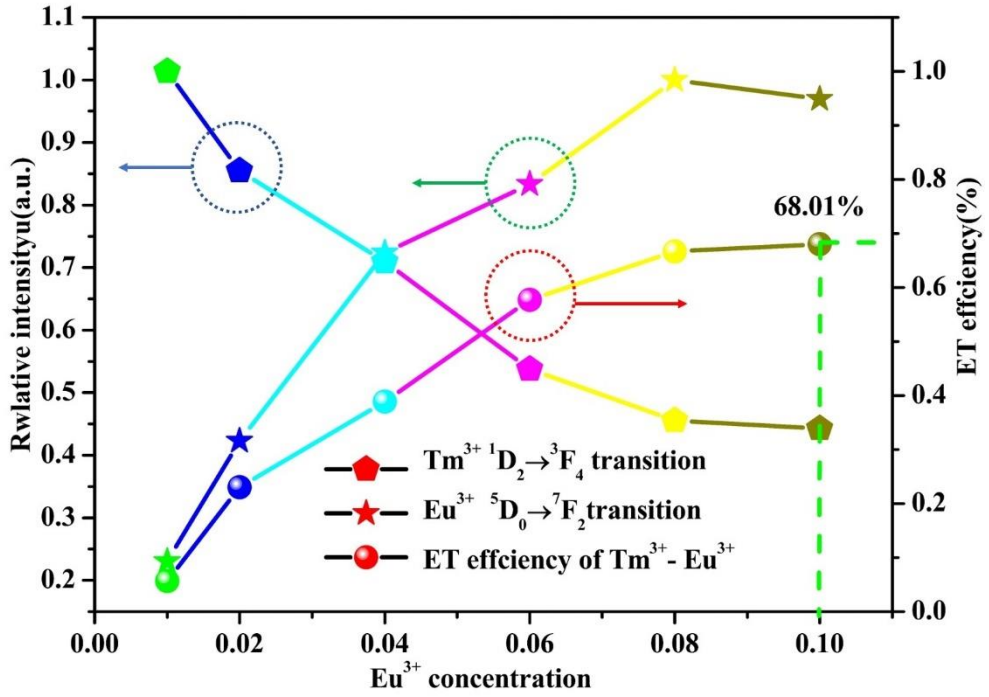

Fig. 11 L. Du et al.

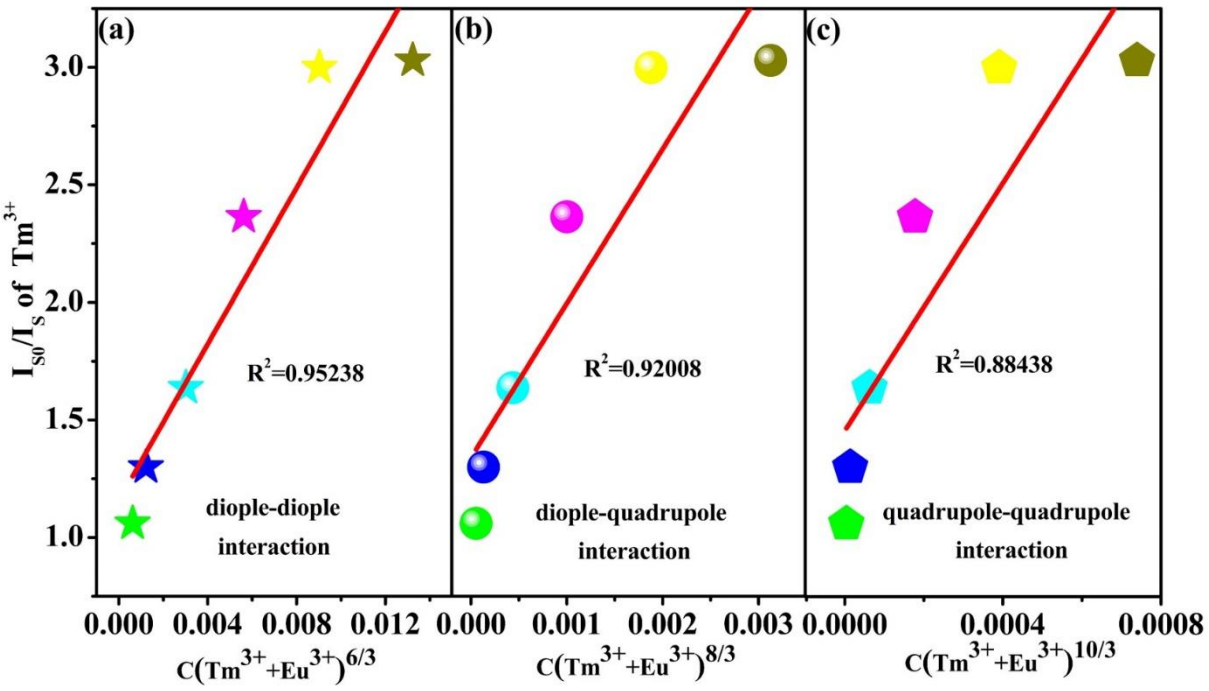

Fig. 12 L. Du et al.

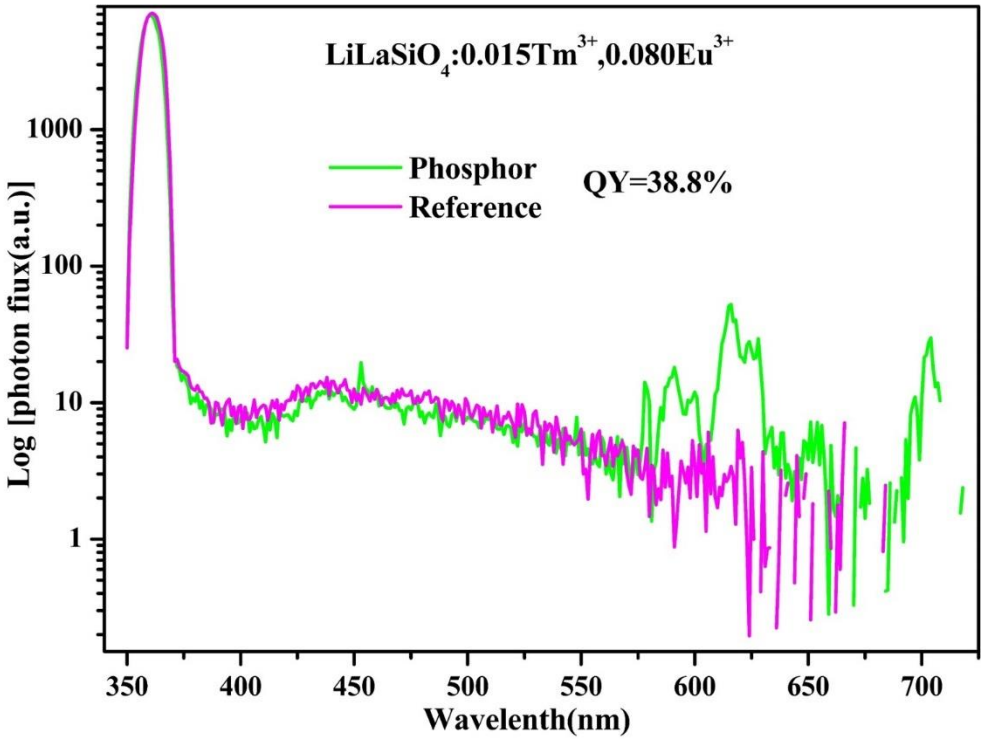

Fig. 13 L. Du et al.

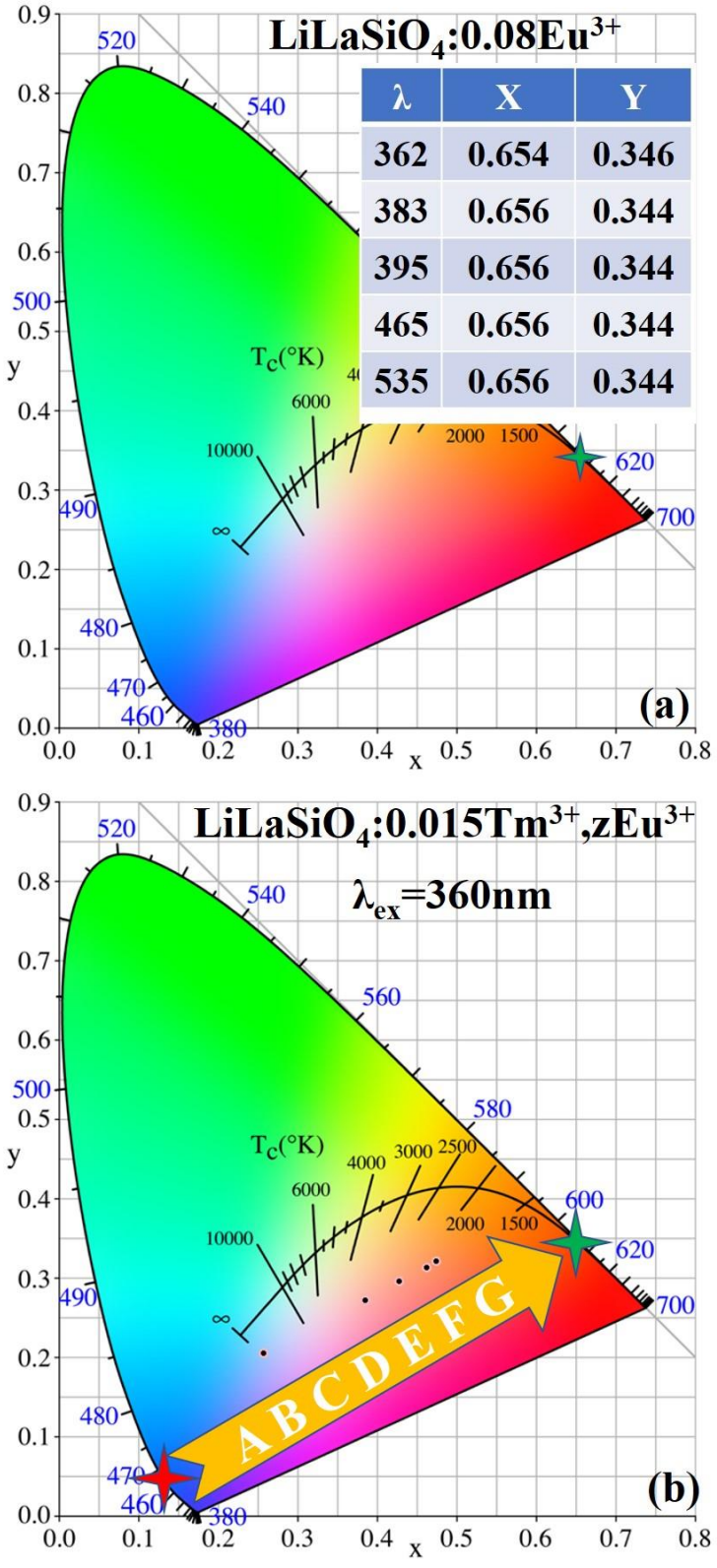

Figures

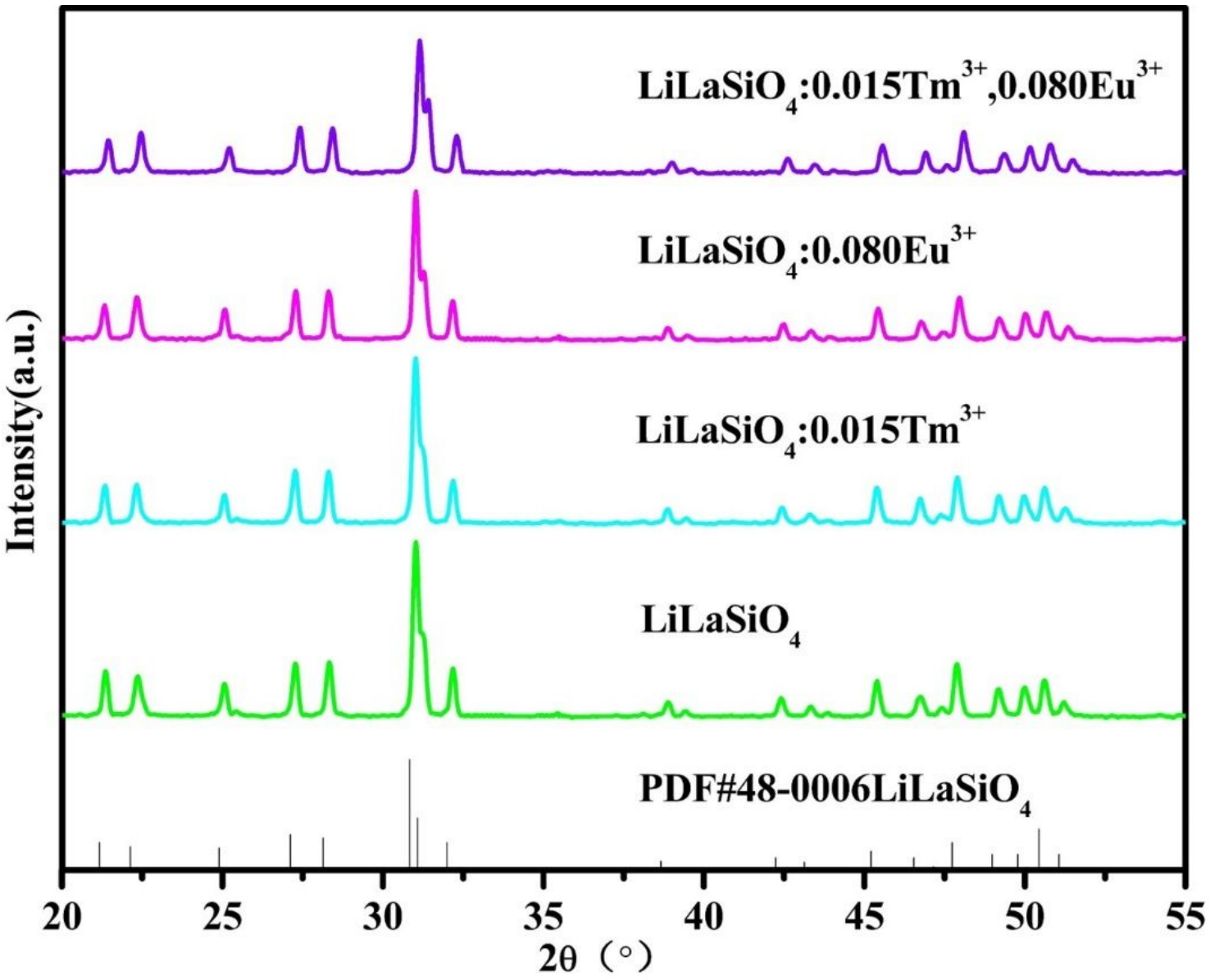

Figure 1

X-ray diffraction patterns of LiLaSiO4:yTm3+, zEu3+ phosphors and the standard card of LiLaSiO4 (JCPDS NO. 48-0006).

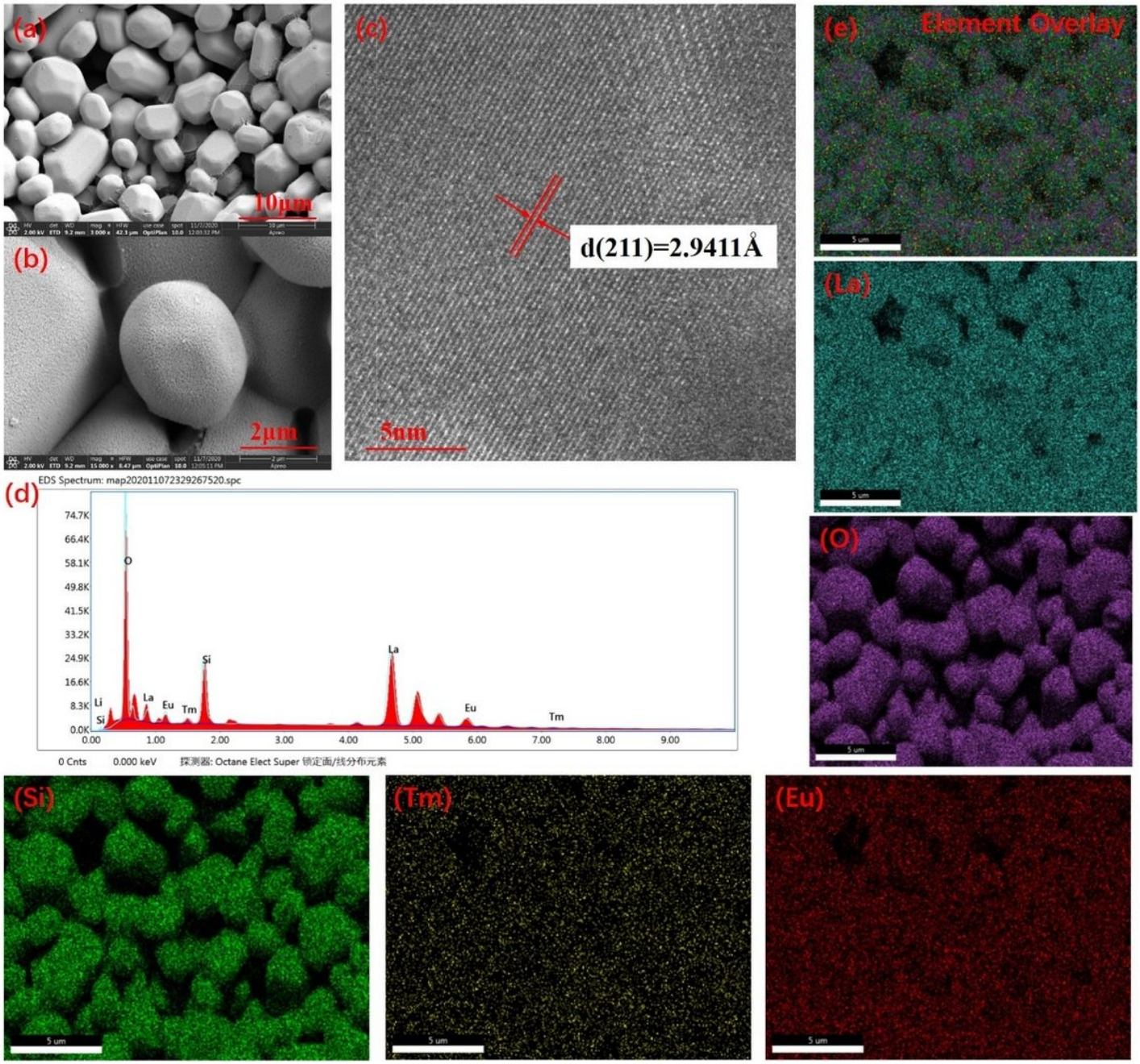

Figure 2

a-b SEM images of LiLaSiO4:0.015Tm3+,0.08Eu3+ phosphor, (c) TEM of LiLaSiO4:0.015Tm3+,0.08Eu3+ phosphor, (d) EDS of LiLaSiO4:0.015Tm3+,0.08Eu3+ phosphor, (e) element distribution of LiLaSiO4:0.015Tm3+,0.08Eu3+ phosphor.

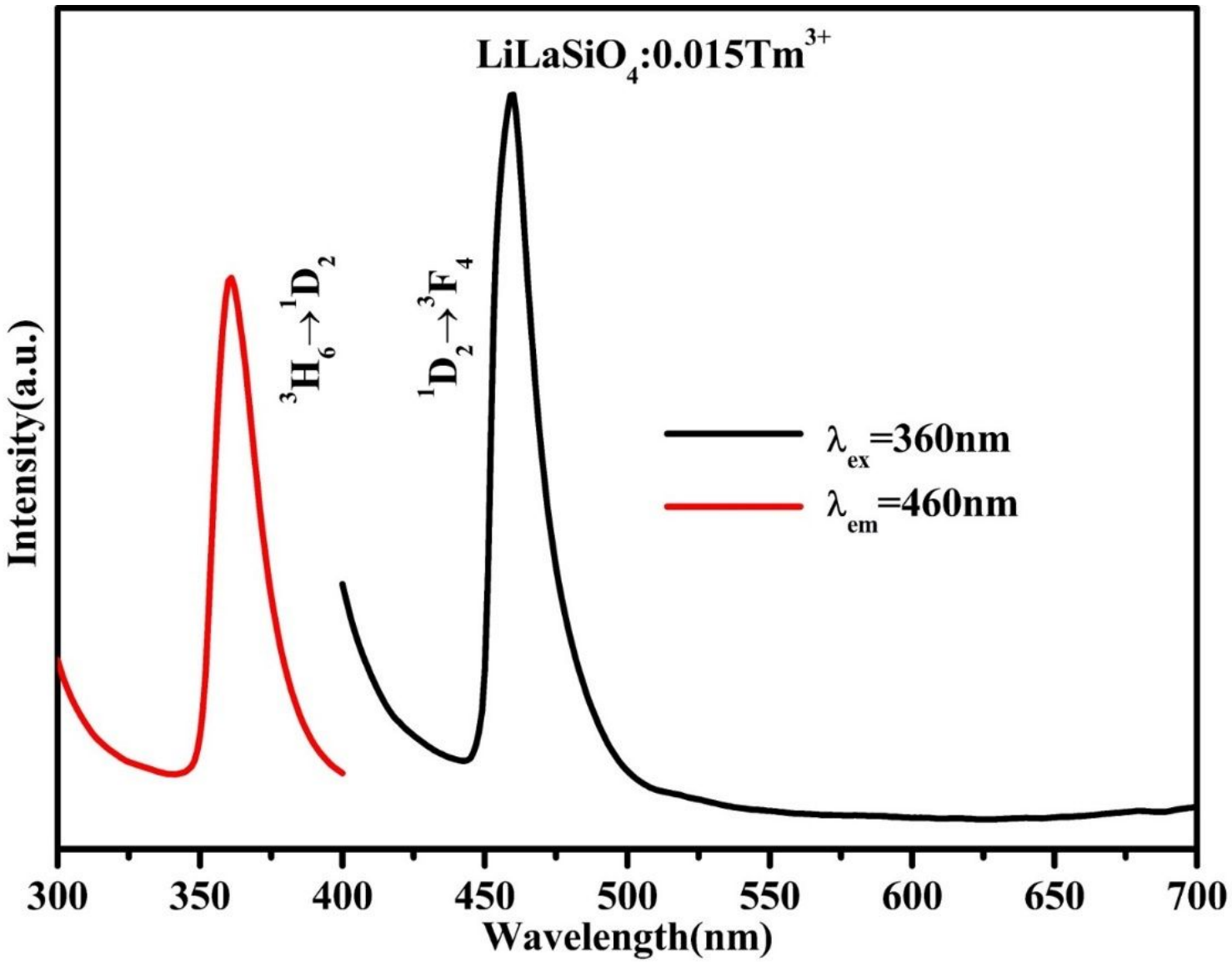

Figure 3

Excitation spectra and Emission spectra of LiLaSiO4:0.015Tm3+ phosphor.

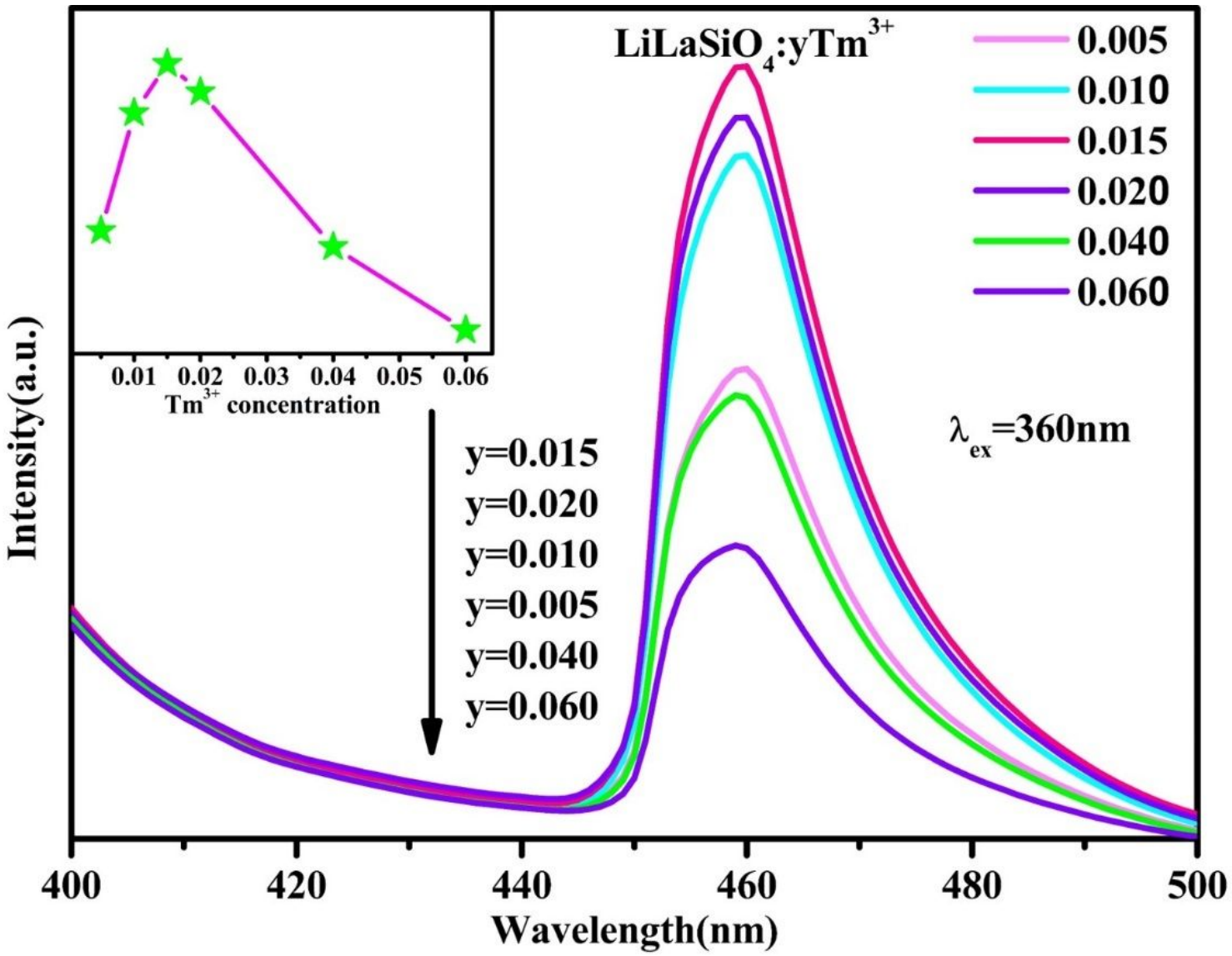

Figure 4

Emission spectra of LiLaSiO4:yTm3+ phosphor.

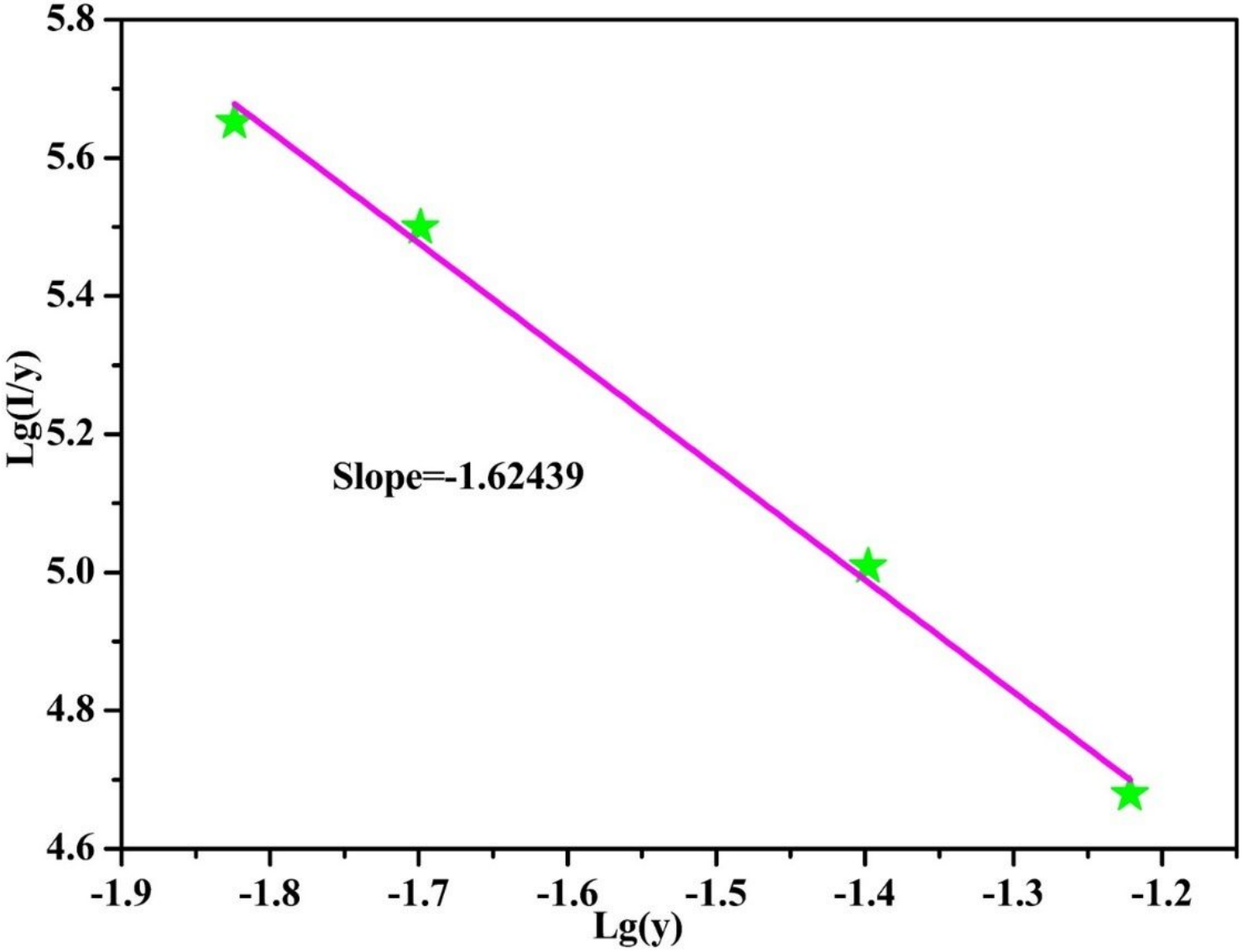

Figure 5

Please see the Manuscript PDF file for the complete figure caption

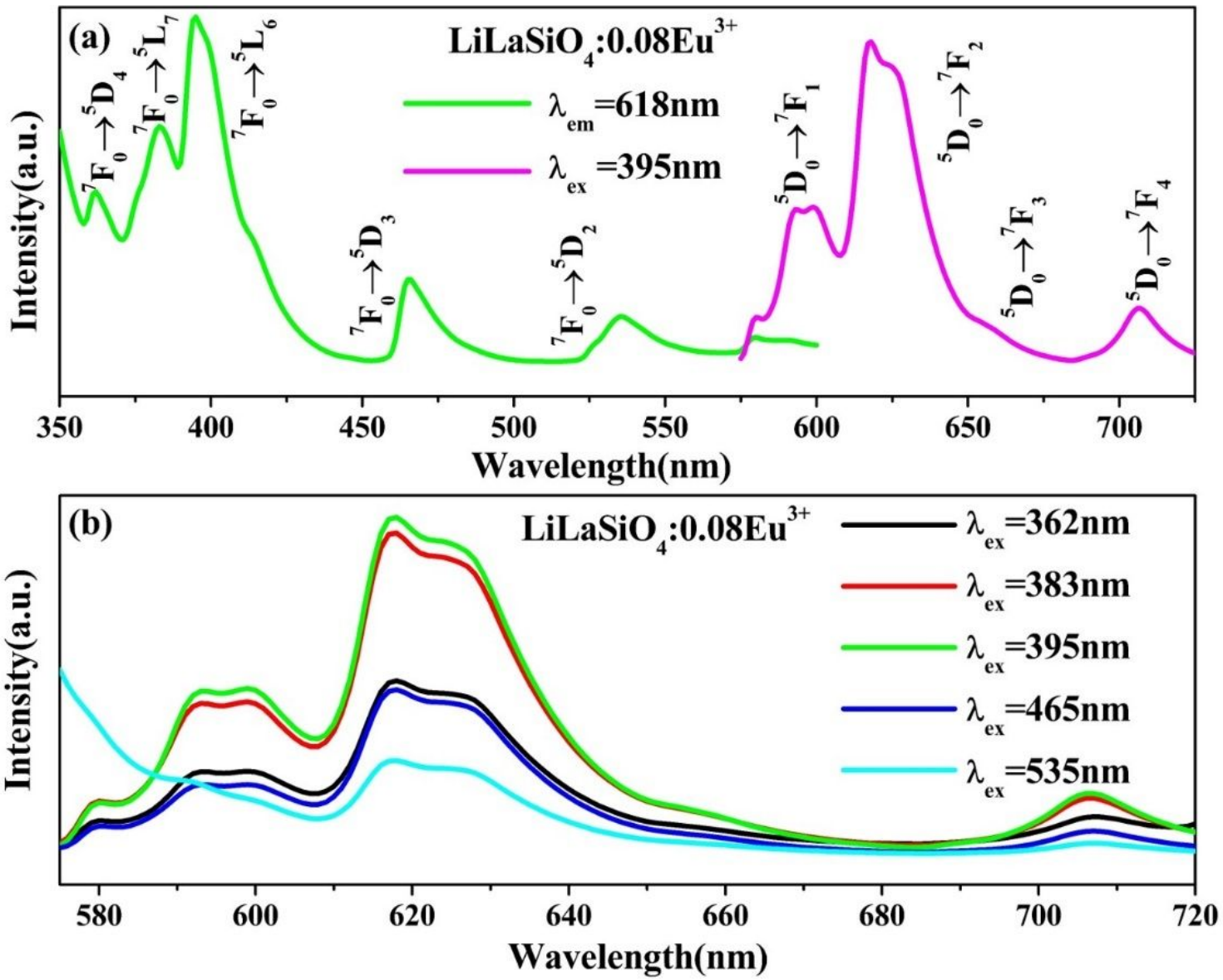

Figure 6

(a) Excitation and emission spectra of LiLaSiO4:0.08Eu3+ phosphor, (b) emission spectra of LiLaSiO4:0.08Eu3+ phosphor at different monitoring wavelength (λex=362, 383, 395 465 and 535nm)

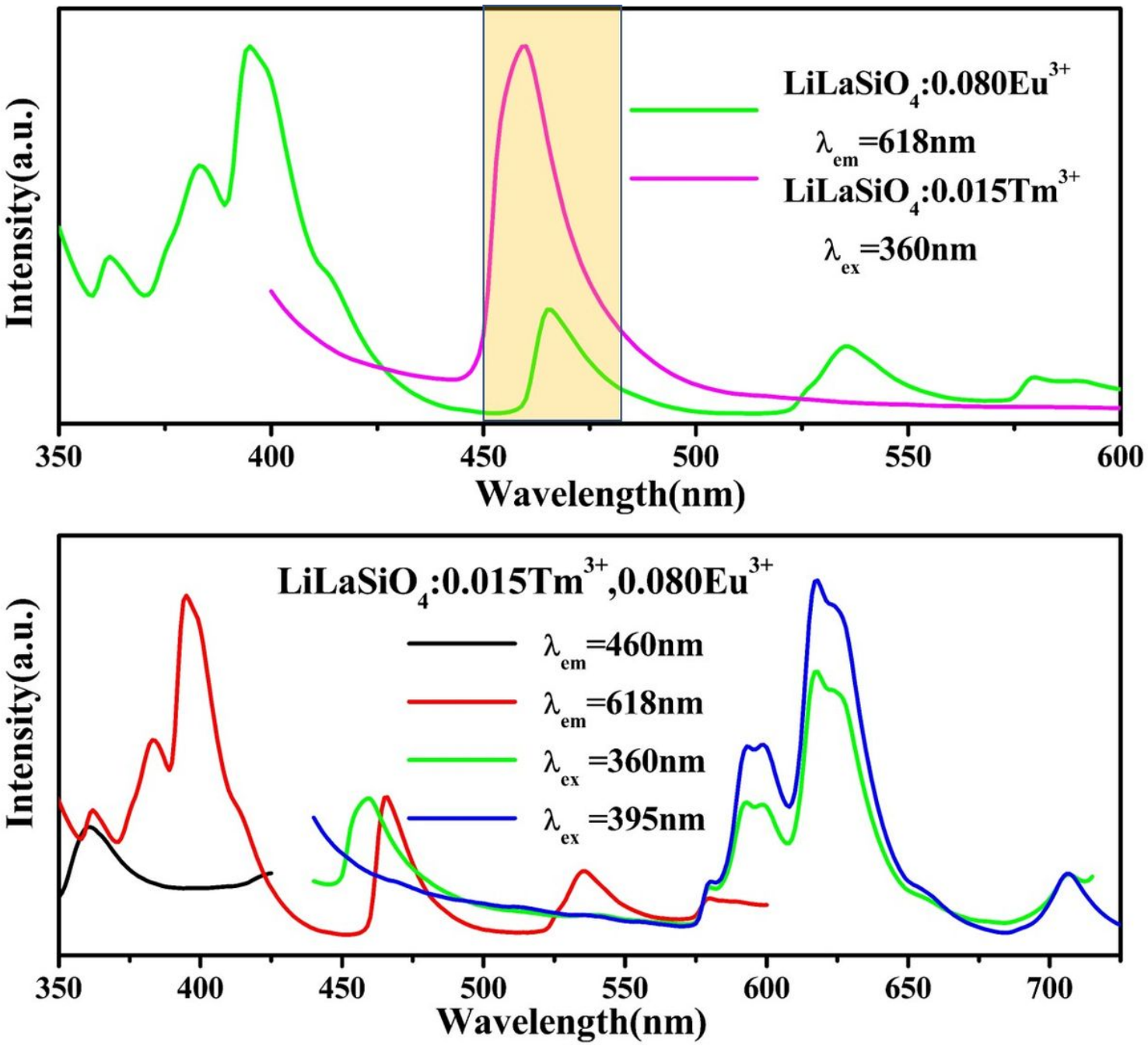

Figure 7

(a) Excitation spectra of LiLaSiO4:0.08Eu3+ phosphor and emission spectra of LiLaSiO4:0.015Tm3+ phosphor, (b) excitation and emission spectra of LiLaSiO4:0.015Tm3+, 0.08Eu3+ phosphor.

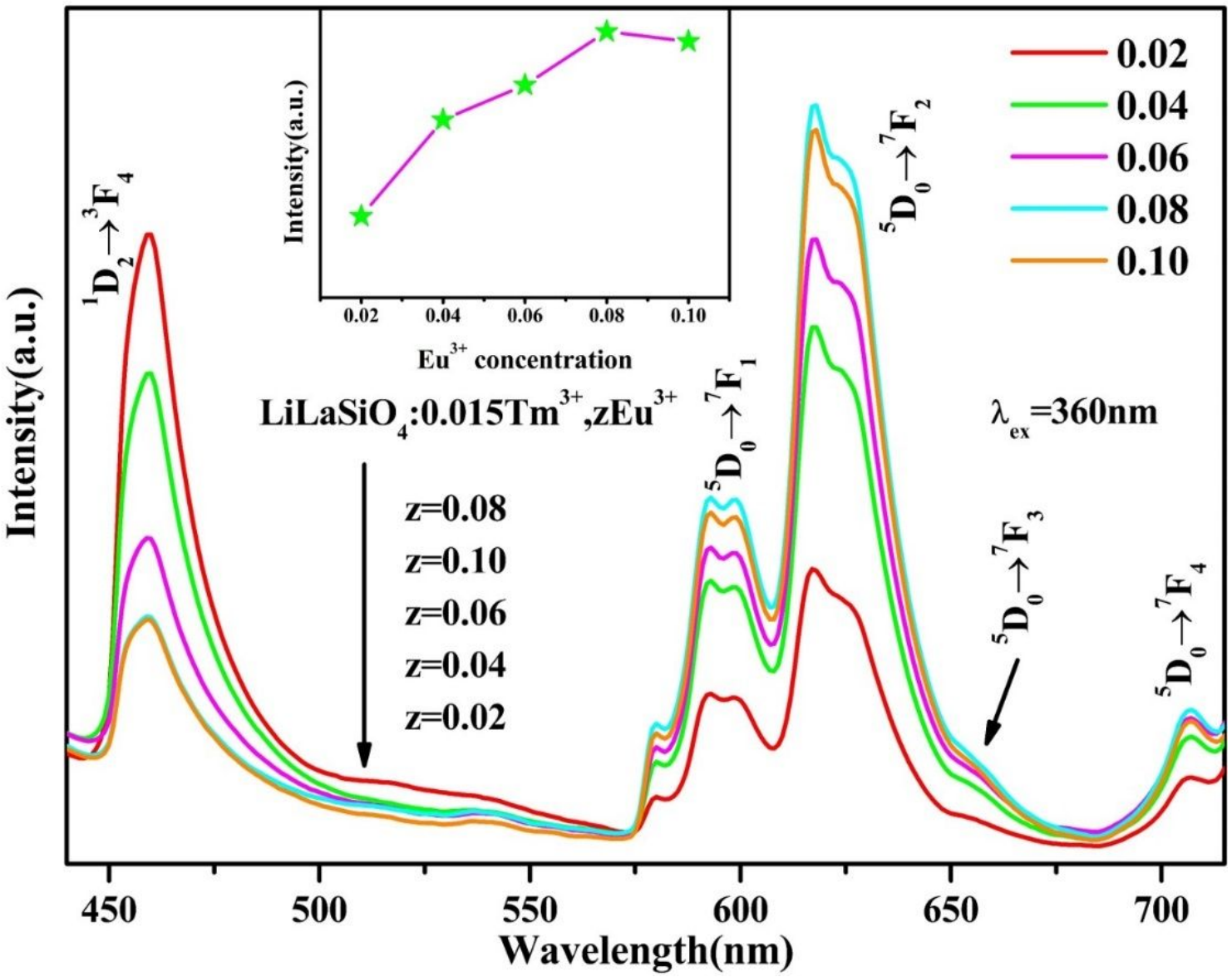

Figure 8

Emission spectra of LiLaSiO4:0.015Tm3+, yEu3+ phosphors.

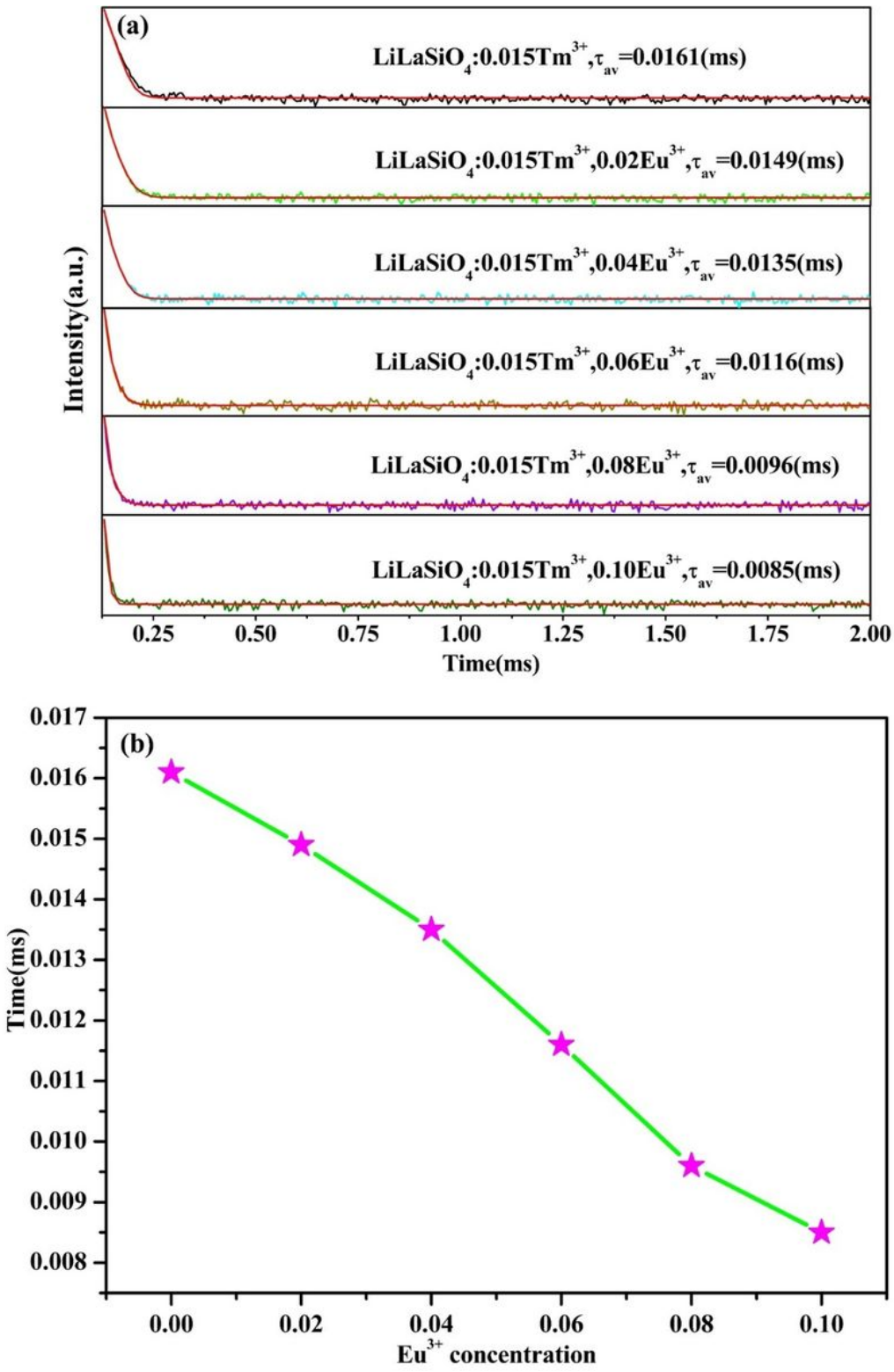

Figure 9

(a) Decay curves of LiLaSiO4:0.015Tm3+, yEu3+ phosphors, (b)variation in decay times of phosphors with different Eu3+ doping rates.

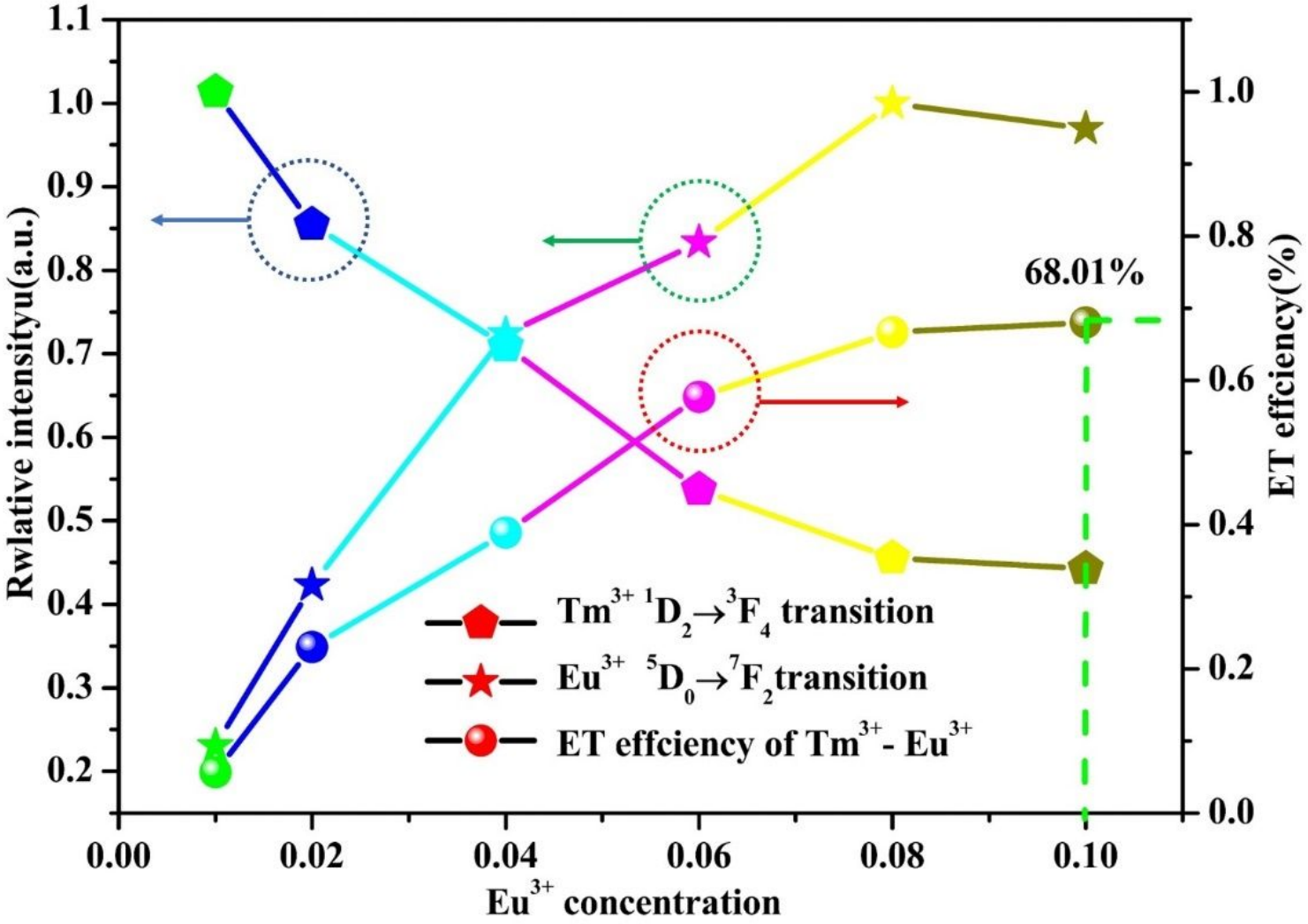

Figure 10

Energy transfer efficiency of Tm3+Eu3+ and changes in luminous intensity of Tm3+ and Eu3+ ions

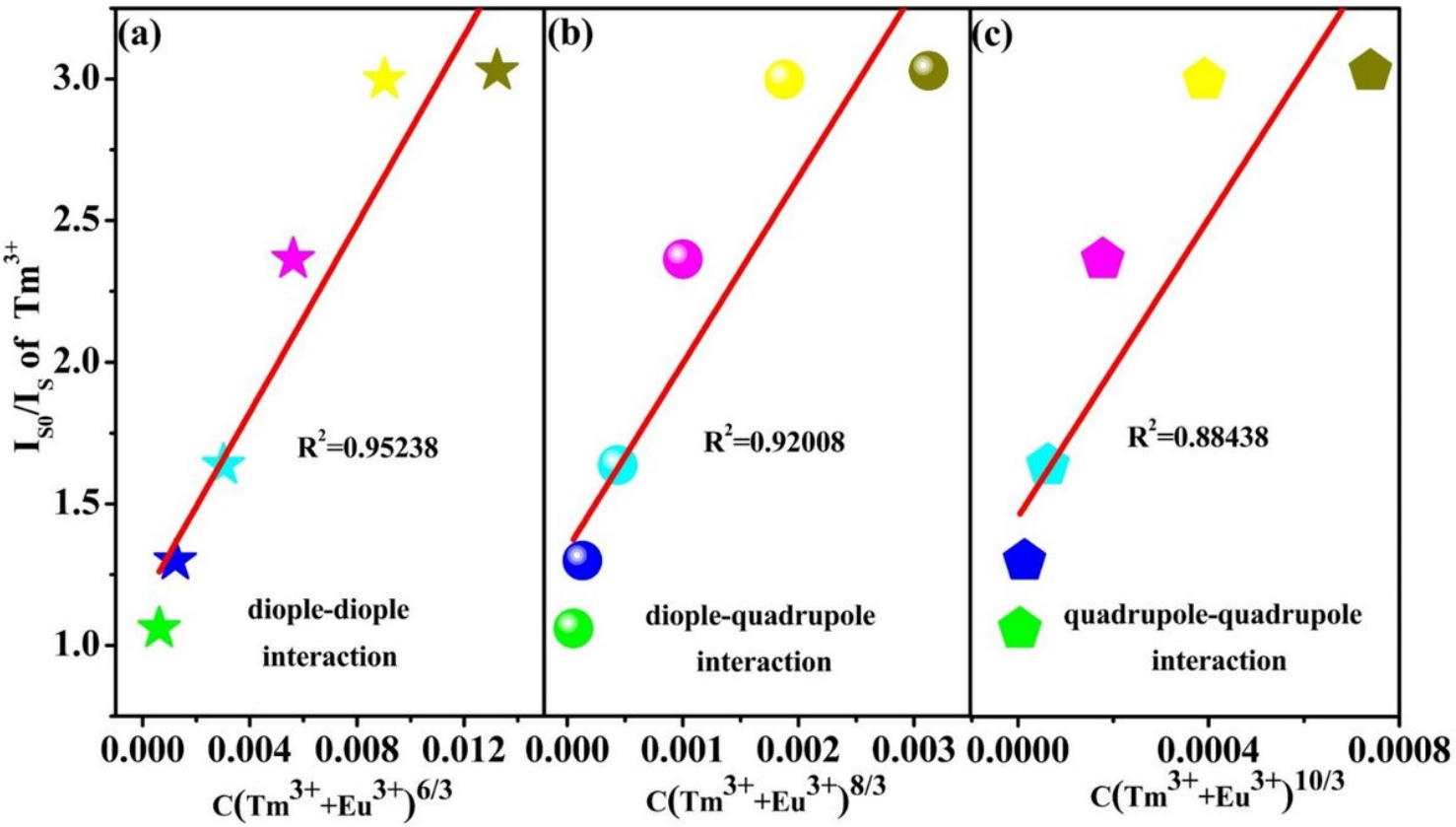

Figure 11

Fitting relationship of IS0/IS of Tm3+ on (a) C(Tb3++Eu3+)6/3, (b) C (Tb3++Eu3+)8/3 and (c)C(Tb3++Eu3+)10/3.

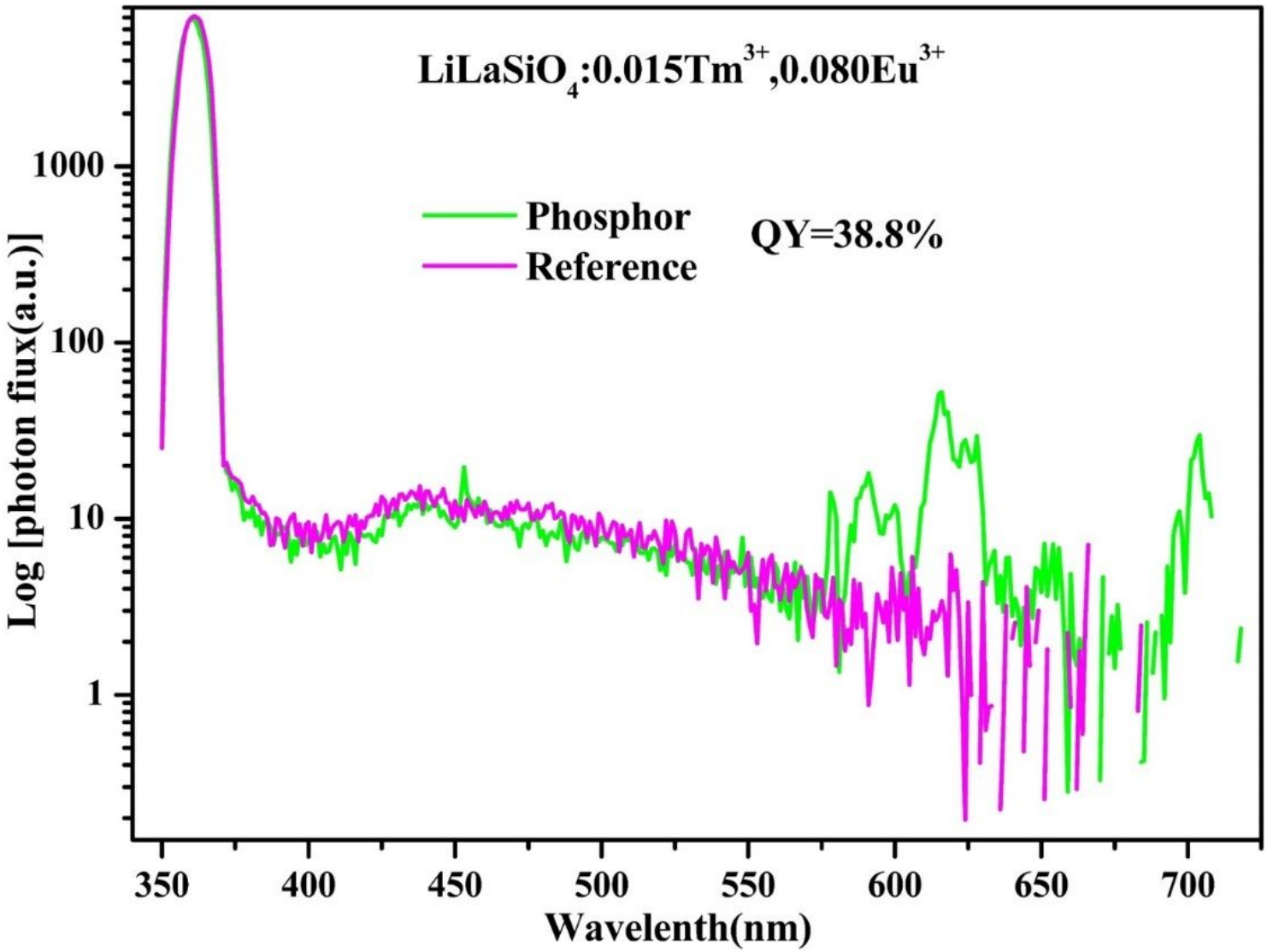

Figure 12

Excitation and emission spectra of LiLaSiO4:0.015Tm3+, 0.08Eu3+ phosphor reference sample for QY measurement

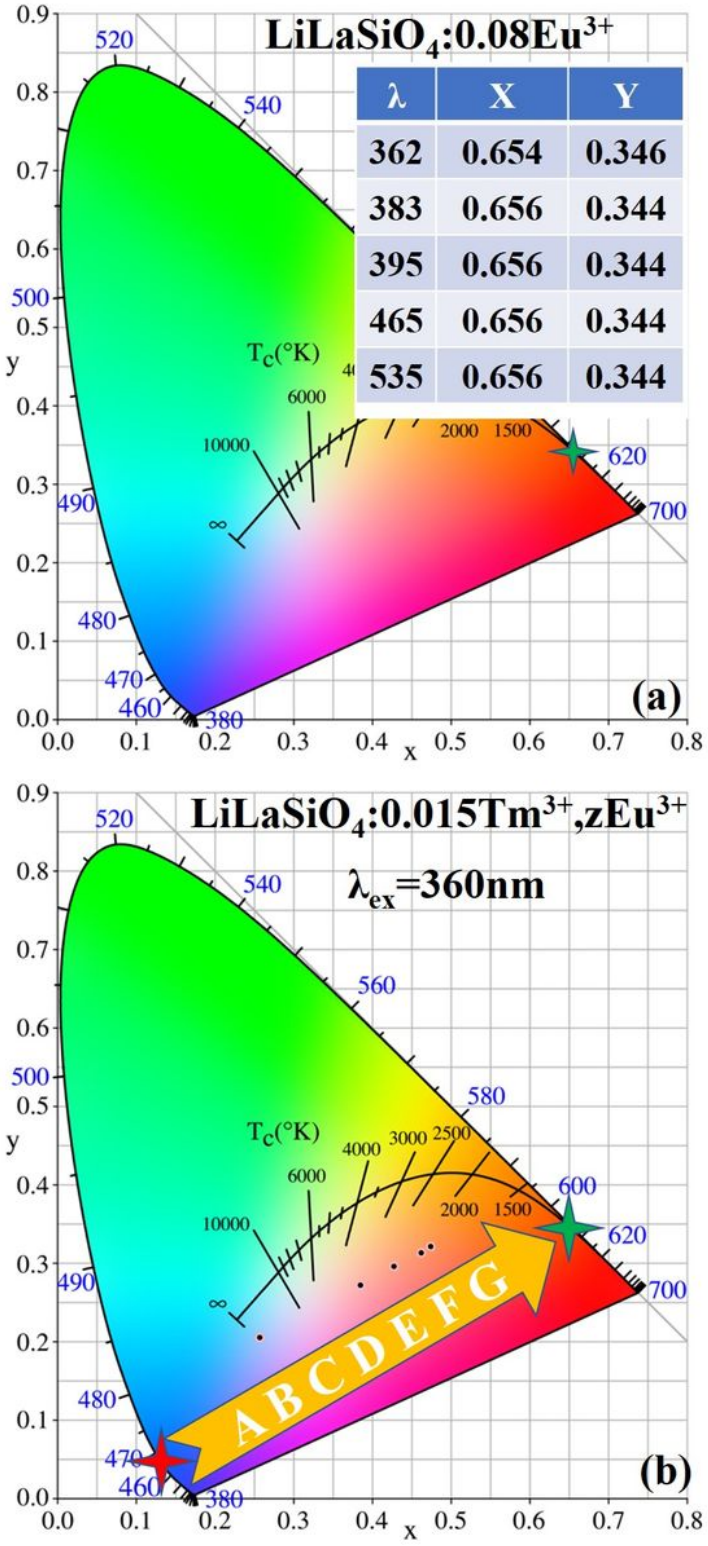

Figure 13

(a) Color coordinates of LiLaSiO4:0.08Eu3+ phosphors at different monitoring wavelength (λex=362, 383, 395 465 and 535nm), (b) color coordinates of LiLaSiO4:0.015Tm3+, yEu3+ phosphors,